Calhoun
Institutional Archive of the Naval Postgraduate School

**Calhoun: The NPS Institutional Archive**

**DSpace Repository**

Theses and Dissertations | 1. Thesis and Dissertation Collection, all items

1970

# Relative performance of different LMFBR lattice configurations under natural circulation.

Newton, John William

Massachusetts Institute of Technology

http://hdl.handle.net/10945/15147

*Downloaded from NPS Archive: Calhoun*

http://www.nps.edu/library

Calhoun is the Naval Postgraduate School's public access digital repository for research materials and institutional publications created by the NPS community. Calhoun is named for Professor of Mathematics Guy K. Calhoun, NPS's first appointed -- and published -- scholarly author.

Dudley Knox Library / Naval Postgraduate School
411 Dyer Road / 1 University Circle
Monterey, California USA 93943

# RELATIVE PERFORMANCE OF DIFFERENT LMFBR LATTICE CONFIGURATIONS UNDER NATURAL CIRCULATION

by

John William Newton

LIBRARY
NAVAL POSTGRADUATE SCHOOL
MONTEREY, CALIF. 93940

# RELATIVE PERFORMANCE OF DIFFERENT LMFBR LATTICE CONFIGURATIONS UNDER NATURAL CIRCULATION

by

John William Newton

B.S., United States Naval Academy
(1969)

SUBMITTED IN PARTIAL FULFILLMENT OF THE
REQUIREMENTS FOR THE DEGREE OF
MASTER OF SCIENCE

at the

MASSACHUSETTS INSTITUTE OF TECHNOLOGY

AUGUST 1970

LIBRARY
NAVAL POSTGRADUATE SCHOOL
MONTEREY, CALIF. 93940



ABSTRACT

RELATIVE PERFORMANCE OF DIFFERENT LMFBR LATTICE CONFIGURATIONS UNDER NATURAL CIRCULATION

by

John William Newton

Submitted to the Department of Nuclear Engineering on August 24, 1970, in partial fulfillment of the requirements for the degree of Master of Science

Analytic comparisons of the performance of LMFBR open-hexagonal, triangular, and square lattice configurations under natural circulation flow conditions were made. Lattices having the same volumetric compositions were compared with respect to reactivity change upon sodium voiding, pressure drop, and linear power output.

A brief study of the relative advantage of the lattices from the standpoint of reactivity change upon sodium voiding of a coolant channel showed that the open-hexagonal lattice was preferable because of its larger coolant-channel radius.

As regards hydraulic and thermal aspects, it was found that core pressure drops and linear power outputs were equivalent for the three lattices under both natural circulation and forced convection, for both laminar and turbulent flow regimes.

Consideration was given to developing more accurate relations for the hydraulic characteristics of the open-hexagonal lattice by modifying the traditional hydraulic diameter concept. Finally, some limitations of the open-hexagonal lattice as compared to the triangular lattice were discussed and necessary areas for future work were identified.

Thesis Supervisor: Michael J. Driscoll
Associate Professor of Nuclear Engineering

Thesis Supervisor: Neil E. Todreas
Assistant Professor of Nuclear Engineering

ACKNOWLEDGEMENTS

The author wishes to express appreciation for the assistance of his thesis supervisors, Dr. M. J. Driscoll and Dr. N. E. Todreas. He is indebted to the National Science Foundation and to the Nuclear Engineering Department of Massachusetts Institute of Technology for a traineeship which made work toward an advanced degree possible. He also wishes to express appreciation to Dianne Bagenski for the assistance given in preparing the final draft of this thesis.

TABLE OF CONTENTS


| | | Page |
|---|---|---|
| Chapter 1 | Introduction | 9 |
| | 1.1 Background | 9 |
| | 1.2 Objectives | 9 |
| | 1.3 Discussion | 9 |
| | 1.4 Choice of Design Restraints and Variables | 13 |
| | 1.5 Synopsis | 14 |
| Chapter 2 | Reactivity Effects of Voided Coolant Channels | 15 |
| | 2.1 Reactivity Effect Components in a Sodium Voided Coolant Channel | 15 |
| | 2.2 Leakage Reactivity Calculations for Open-hexagonal and Triangular Lattices | 16 |
| Chapter 3 | Expressions for and Comparison of Mass Flow Rates, Pressure Drops and Linear Power Output for Different LMFBR Lattice Configurations | 21 |
| | 3.1 Discussion | 21 |
| | 3.2 Procedure for Calculation of Core and Spacer Pressure Drop | 22 |
| | 3.3 Theoretical Core and Spacer Pressure Drop | 23 |
| | 3.4 Empirical Spacer Pressure Drop | 28 |
| | 3.5 Mass Flow Rate and Linear Power Output in Steady-state Thermal Circulation | 31 |
| | 3.6 Comparison of Linear Power Output in Open-hexagonal, Triangular, and Square Lattices | 32 |

| | | Page |
|---|---|---|
| Chapter 4 | Example Calculations of Mass Flow Rate, Pressure Drop, and Linear Power Output | 37 |
| | 4.1 Discussion | 37 |
| | 4.2 Calculations of Flow Parameters and Theoretical Spacer Pressure Drop in the Open-hexagonal Flow Cell | 38 |
| | 4.3 Calculations of Flow Parameters and Theoretical Spacer Pressure Drop in the Triangular Flow Cell | 42 |
| | 4.4 Empirical Spacer Pressure Drop for the Triangular and Open-hexagonal Lattices | 48 |
| | 4.5 Linear Power Output for the Open-hexagonal Lattice | 53 |
| Chapter 5 | Equivalent Diameter for the Open-hexagonal Lattice | 58 |
| | 5.1 Definition of Equivalent Diameter | 58 |
| | 5.2 Conditions for a Laminar Flow Region in the Open-hexagonal Flow Cell | 58 |
| | 5.3 Calculation of Laminar Sublayer Thickness in Turbulent Flow | 61 |
| Chapter 6 | Summary and Conclusions | 64 |
| | 6.1 Summary | 64 |
| | 6.2 Discussion | 65 |
| | 6.3 Future Work | 68 |
| | 6.4 Conclusion | 70 |
| Appendix A | Linear Power Relationship for Natural Circulation in a Reactor | 71 |
| Appendix B | Derivation of Hydraulic Diameters as Functions of Pitch and Diameters of Fuel Pins | 78 |

| | | Page |
|---|---|---|
| Appendix C | Lattice Parameters | 80 |
| Appendix D | Relative Linear Power Output for Various Lattice Configurations Under Forced Circulation | 91 |
| Appendix E | References | 94 |
| Appendix F | Nomenclature | 96 |

# LIST OF FIGURES


| | | Page |
|---|---|---|
| 1.1 | Lattice configurations | 10 |
| 1.2 | Unit cell configurations | 11 |
| 3.1 | Pressure loss coefficients | 24 |
| 3.2 | Flow areas in a coolant cell | 26 |
| 3.3 | Ratio of friction factors in non-circular and circular channels | 27 |
| 3.4 | Drag coefficients for honeycomb grid spacers | 30 |
| 3.5 | Illustrative graph of solutions for natural circulation operating conditions | 33 |
| 4.1 | Example natural circulation operating conditions | 57 |
| A.1 | Thermal circulation driving heads | 72 |
| A.2 | Illustrative graph of solutions for natural circulation operating conditions | 76 |
| A.3 | Comparison of driving forces in forced and natural convection | 77 |
| C.1 | Lattice parameters | 86 |
| C.2 | Core subassembly configuration | 88 |

# LIST OF TABLES


| | | Page |
|---|---|---|
| IV.1 | Flow Parameters for the Open-hexagonal Lattice | 41 |
| IV.2 | Pressure Drop in the Open-hexagonal Lattice Flow Cell | 43 |
| IV.3 | Flow Parameters for the Triangular Lattice | 46 |
| IV.4 | Pressure Drop in the Triangular Lattice Flow Cell | 49 |
| IV.5 | Flow Parameters and Pressure Drop in the Spacer Region for the Triangular Lattice Flow Cell | 51 |
| IV.6 | Mass Flow Rates per Unit Flow Area and Total Friction Pressure Drop as Functions of a Calculated $f_s$ in the Open-hexagonal and Triangular Flow Cells | 56 |
| VI.1 | Assumed and Calculated Core Parameters for Various Lattices | 69 |
| C.1 | Current and Proposed LMFBR Parameters | 81 |
| C.2 | Lattice Parameters | 85 |

# Chapter 1

## Introduction

### 1.1 Background

In liquid-metal cooled fast-breeder reactors an area of particular concern is that of loss of heat removal capability and subsequent coolant boiling. The designs for most large LMFBR's of the future include the capability for the removal of generated heat by natural circulation in the event of loss of pumping power. Most of these designs were based on the use of triangular pitch fuel pin lattices.

### 1.2 Objectives

The objective of this thesis is to determine the relative performance of different LMFBR lattice configurations under natural circulation with respect to the power output which could be attained during normal operation and with respect to safety considerations in the event of loss of primary pumping power in a pumped circulation system. Figures 1-1 and 1-2 describe the lattice configurations under consideration.

### 1.3 Discussion

Advantages of natural circulation operation include:

1. At full power operation primary pumps would be eliminated, a factor which would reduce cost of hardware and eliminate the concern of a loss of pumping power.

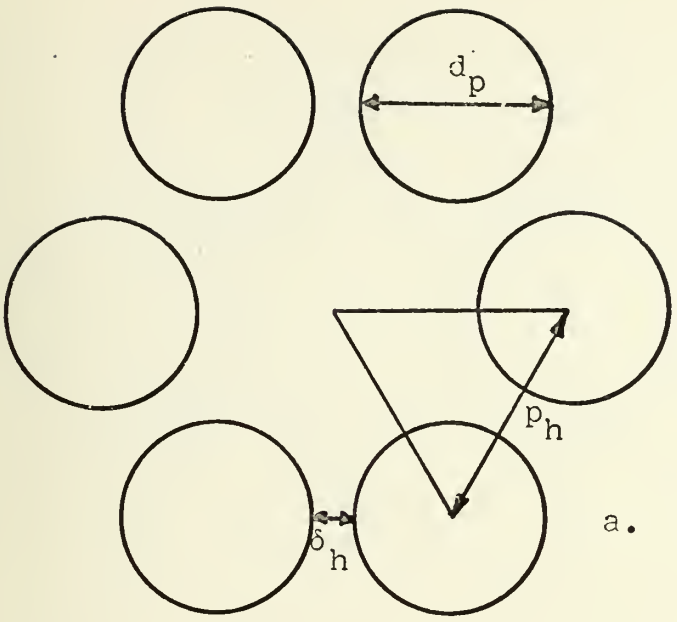


a. Open-hexagonal lattice

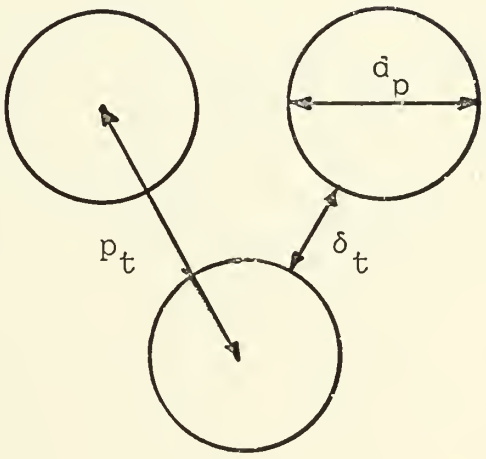


b. Triangular lattice

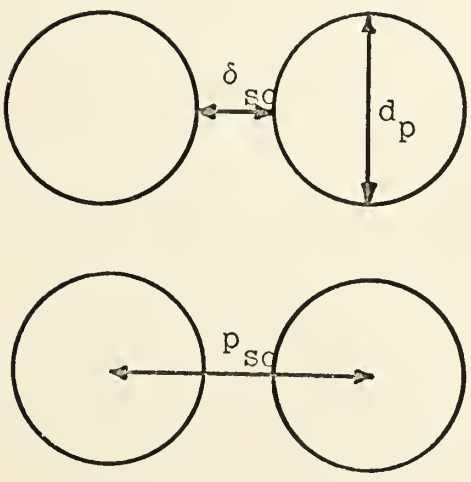


c. Square lattice

Fig. 1.1. Lattice configurations

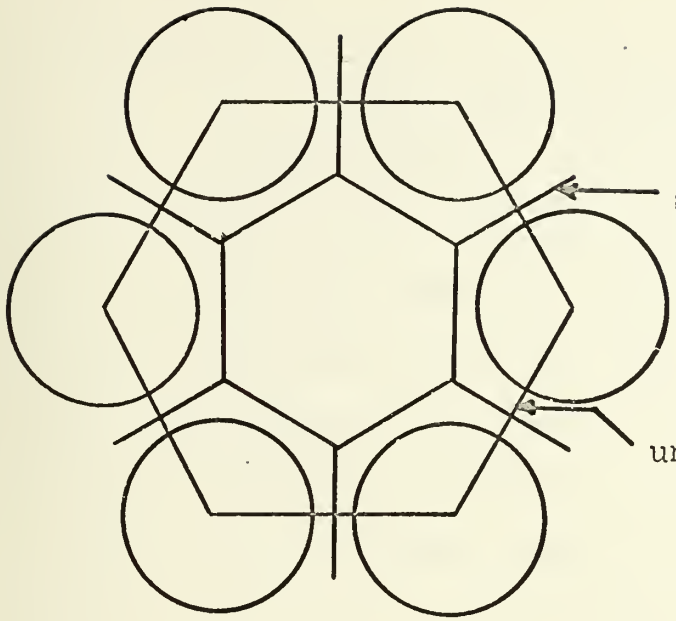


a. Open-hexagonal cell

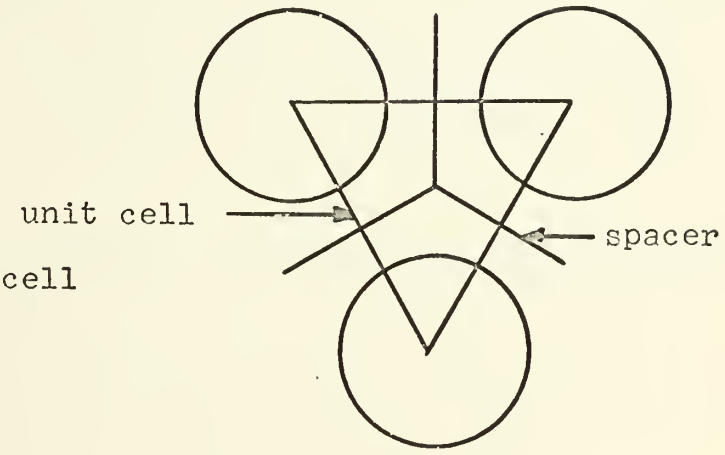


b. Triangular cell

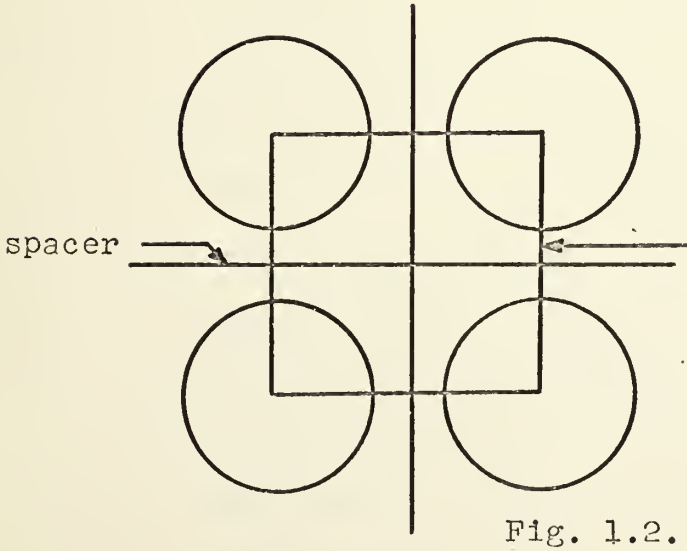


c. Square cell

Fig. 1.2. Unit cell configurations

2. At full power operation a natural circulation system would, to some extent, be self-regulating; for a given channel, as power increases/decreases, the core inlet and outlet temperature difference and the coolant mass flow rate would increase/decrease. The parallel channel problem requires further investigation, however.

3. In a pumped system natural circulation would serve as a safety measure in that the loss of primary pumping power would not result in coolant boiling and burnout since a sufficiently large natural flow could carry away the heat quickly enough.

Disadvantages of natural circulation operation include:

1. The plant will have to operate at a lower power output than would a plant with primary coolant pumps if design variables cannot adequately be optimized within various constraints.

2. The design of the system would necessitate placing the intermediate heat exchanger far above the core in order to achieve the necessary height between the core and the heat exchanger for a desired thermal driving potential. In this position the intermediate heat exchanger could complicate access to the core from above and would necessitate a larger (taller) outer containment structure.

## 1.4 Choice of Design Constraints and Variables

The loop-type system was chosen as the primary coolant system. Since the reactor system needs a high thermal driving head in order to attain the desired coolant flow rate, the intermediate heat exchanger needs to be above the core at a height which cannot practically be designed into a pot-type system. However, the pot-type system, through the thermal inertia of its large pool of sodium, provides ample margin for core cooling following loss of pumping power.

Sodium is by far the coolant of choice for recent LMFBR designs. Thus, in this study liquid sodium was chosen as the coolant.

The type of spacer system chosen for the open-hexagonal lattice was the grid system. Wire-wrap spacers would probably be more practical economically[1], but with the center of the open-hexagonal lattice open, each rod would have support only from three wires in one complete spiral instead of support from six wires as in a triangular pitch. The grid spacer was chosen in order that the open-hexagonal system would have the most and sufficient support against vibration.

In the comparison of the three lattices several variables will be examined. Under natural circulation the linear power output depends on a combination of core temperature rise, fuel pin diameter and pitch, fuel pin

length, and the effective heat exchanger height to primary coolant system length ratio. Combinations of the variables will be discussed with the use of typical values of current LMFBR fluid and mechanical parameters.

## 1.5 Synopsis

The comparison of the LMFBR lattices will first be examined from the standpoint of the additional leakage reactivity resulting from the heterogeneity of the core using the different lattices. An examination of the relative mass flow rates, core pressure drops, and linear power outputs will then be made followed by an example calculation of these quantities. In addition a more applicable expression for hydraulic diameter will be sought for an open-hexagonal lattice. Finally, conclusions and recommendations will be proposed.

# Chapter 2

## Reactivity Effects of Voided Coolant Channels

### 2.1 Reactivity Effect Components in a Sodium Voided Coolant Channel

When a coolant channel is voided of sodium, a change in reactivity occurs. This reactivity change consists of three first order components: a change in the number of neutrons captured, a shift in the neutron spectrum, and leakage of neutrons. Detailed discussion of the total sodium-void effect may be found in publications by Hummel and Okrent[2] and Monroe[3].

Most calculations of the leakage component of the change in reactivity are based on the assumption that the reactor is homogeneous. In this chapter a rough calculation of the additional leakage reactivity effect due to the heterogeneity of the core will be made. For a more detailed discussion of the leakage component of sodium-void reactivity in heterogeneous cores, the reader is refered to a study made by Lacapelle[4] whose method was based on the work of Benoist[5]. The leakage component of the overall reactivity change will be compared in the open-hexagonal and triangular lattices showing that the larger hole of the open-hexagonal cell results in a greater negative reactivity than does the hole in the triangular cell. The calculations used in the comparison are based on formulations derived in Behren's original paper "The Effect of Holes in a Reacting Material on the Passage of Neutrons"[6].

## 2.2 Leakage Reactivity Calculations for Open-hexagonal and Triangular Lattices

Comparing Behren's Eq. (8) and Eq. (10) for closely spaced, interacting holes in a medium having a long mean free path we have

$$\frac{L^2}{L_0^2} = 1 + 2\phi + \phi^2 + \frac{Qr_{hy}\phi}{\lambda} \quad , \tag{2-1}$$

where

- $\phi$ is the volume ratio of the holes to the material of the reactor,
- $Q$ is a function of the shape of the hole,
- $\lambda$ is the mean free path in the solid,
- $r_{hy} \equiv \frac{2\phi\nu}{S}$ is the nuclear hydraulic radius of the cell,
- $\nu$ is the volume of the cell of material surrounding each hole,
- $S$ is the surface area of each hole,
- $L_0^2$ is the mean square direct distance travelled by a neutron in the course of N collisions in a homogeneous medium,
- $L^2$ is the mean square direct distance travelled by a neutron in the course of N collisions in a medium with holes,

The change in reactivity is given by

$$\frac{\delta k}{k} = -\left(\frac{\delta D}{D_{Hom}}\right)(k_\infty - 1)/k_\infty \ . \tag{2-2}$$

The definition of diffusion length gives

$$\frac{L^2}{L_0^2} = \frac{D\Sigma_a^0}{D_0\Sigma_a} = (1 + \phi)\frac{D}{D_0} \ , \tag{2-3}$$

since

$$\Sigma_a = \frac{\Sigma_a^0 V_{fuel}}{V_{tot}} = \frac{\Sigma_a^0 V_{fuel}}{(V_{fuel} + V_{hole})} = \frac{\Sigma_a^0}{(1 + \phi)} \quad . \qquad (2\text{-}4)$$

Equating Eqs. (2-1) and (2-3)

$$(1 + \phi)\frac{D}{D_0} = (1 + \phi)^2 + \frac{Qr_{hy}\phi}{\lambda}$$

or

$$D = D_0(1 + \phi) + \frac{Qr_{hy}\phi}{3(1 + \phi)} \quad . \qquad (2\text{-}5)$$

The change in the diffusion coefficient is

$$\delta D = D - D_{Hom} = \frac{Qr_{hy}\nu_{hole}}{3} \qquad (2\text{-}6)$$

where

$D_{Hom}$ is the homogeneous value of the diffusion coefficient

$\nu_{hole} = \frac{\phi}{1 + \phi}$ is the volume fraction of holes

For a first approximation we will assume that the cells in our theoretical core are cylindrical. The volume of each cylindrical hole will be set equal to the actual volume of coolant channel associated with a cell, and the volume of fuel material surrounding each hole will be set equal to the actual volume of fuel material associated with a cell. Refer to Fig. 1.2 for the unit cell configurations chosen. Note

that the cells are based on the coolant channel and not on a fuel rod as is the more common convention. When this approximation is made, the nuclear hydraulic radius, $r_{hy}$, is the same as the actual radius of the equivalent cylindrical coolant cell.

Refer to Fig. 1.1.a for a definition of parameters needed to find the hydraulic radius of the open-hexagonal cell:

$$A_{hole} = A_{tot} - A_{fuel} ,$$

$$\pi(r_{hy})_h^2 = \frac{6\sqrt{3}}{4} p_h^2 - \frac{4\pi}{8} d_p^2 ,$$

$$(r_{hy})_h = \frac{1}{2}\left(\frac{6\sqrt{3}}{\pi} p_h^2 - \frac{4}{2} d_p^2\right)^{1/2} . \qquad (2\text{-}7)$$

Refer to Fig. 1.1.b for the hydraulic radius of the triangular lattice:

$$A_{hole} = A_{tot} - A_{fuel} ,$$

$$\pi(r_{hy})_t^2 = \frac{\sqrt{3}}{4} p_t^2 - \frac{\pi}{8} d_p^2 ,$$

$$(r_{hy})_t = \frac{1}{2}\left(\frac{\sqrt{3}}{\pi} p_t^2 - \frac{1}{2} d_p^2\right)^{1/2} . \qquad (2\text{-}8)$$

Since $p_h = (2/3)^{1/2} p_t$ , then

$$(r_{hy})_h = \frac{2}{2}\left(\frac{\sqrt{3}}{\pi} p_t^2 - \frac{1}{2} d_p^2\right)^{1/2} = 2(r_{hy})_t . \qquad (2\text{-}9)$$

Inserting Eq. (2-6) into Eq. (2.2):

$$\frac{\delta k}{k} = -\left(\frac{Q r_{hy} \nu_{hole}}{3 D_{Hom}}\right)\left(\frac{k_\infty - 1}{k_\infty}\right) . \qquad (2\text{-}10)$$

Using the following typical values for an open-hexagonal and a triangular lattice:

$Q = 4/3$ (as tabulated in ref. (6)),

$\nu_{hole} = 1 - \nu_{fuel} = 0.528$,

$p_t = 0.416$ in.,

$p_h = 0.340$ in.,

$d_p = 0.300$ in.,

$D_{Hom} = 4$ cm $= 1.57$ in. for a voided core,

$k_\infty = 1.5$,

the ratio of reactivity changes is

$$\frac{(\delta k/k)_h}{(\delta k/k)_t} = 2 .$$

Solving for the reactivity changes:

$$(\delta k/k)_t = -0.0056 = -\$1.70$$

$$(\delta k/k)_h = -0.0112 = -\$3.40$$

using $\beta = 0.0033 \equiv \$1.00$.

For a square lattice with

$\nu_{hole} = 0.528$

$d_p = 0.300$ in.

$p_s = 0.388$ in.

$$\frac{(\delta k/k)_h}{(\delta k/k)_{sq}} = 1.42$$

and

$$(\delta k/k)_{sq} = -\$2.40 \quad .$$

From the above calculations we can see that the open-hexagonal lattice results in a higher negative reactivity from leakage in a voided coolant channel than do triangular or square lattices of the same volume fraction of fuel. Because of its higher negative reactivity the open-hexagonal lattice is preferable to both the triangular and the square lattices from the standpoint of keeping the effective increase in multiplication factor as low as possible upon sodium voiding of coolant channels.

In the next chapter the relative mass flow rates, core pressure drops, and linear power outputs of the three lattices will be compared. These comparisons will be used in determining which lattice is preferable from hydraulic and power removal aspects.

# Chapter 3

## Expressions for and Comparison of Mass Flow Rates, Pressure Drops and Linear Power Output for Different LMFBR Lattice Configurations

### 3.1 Discussion

As was seen in Chapter 2, the hexagonal lattice proved to be more advantageous than a triangular or square lattice from a leakage reactivity standpoint. In this chapter the three lattices will be compared with respect to some hydraulic and power aspects to see if the larger hole of the open-hexagonal lattice renders it preferable to both the square and triangular lattices. In the present chapter the three lattices will be compared on an equivalent basis, namely, equal rod size and fuel volume fraction, with respect to pressure drops and linear power output. It will be assumed that all fluid properties are equal for the three lattices.

As will be seen in the numerical examples of Chapter 4, the core pressure drops of the three lattice arrangements are essentially the same for equal fuel volume fraction and equal coolant velocities. The only differences in pressure drop are due to the differences in spacer arrangement of the different lattices, and these differences are small. Therefore, these small pressure drop differences can be neglected in a first order approximation of the relative linear power output for the three lattice arrangements. However, in the

calculation of the absolute linear power output for any given lattice, the spacer pressure drop contribution to the total core pressure drop cannot be neglected since it constitutes as much as 45% of the total core pressure drop.

## 3.2 Procedure for Calculation of Core and Spacer Pressure Drop

The total pressure loss, $\Delta P_T$, through the reactor core, hence, through a unit cell flow path in the core, consists of three factors: pressure loss at bundle entrance and exit, $\Delta P_E$; frictional pressure loss without spacers, $\Delta P_R$; pressure loss due to spacers, $\Delta P_S$. It will be assumed that pressure loss at the bundle entrance and exit will be equal for all three lattices. This assumption is based on the fact that the entrance and exit openings are of equal total cross sectional area for the cores containing the different lattices and that the coolant velocities in the three cores are equal. By using equations similar to Eqs. (3-1) and (3-2), one can find that the entrance and exit losses for the different cores are the same.

Since there is no experimental data on pressure drops through open-hexagonal rod bundles with and without spacer devices known to the author, the approach for calculating the semi-empirical pressure drop through an open-hexagonal lattice will be as follows. Tong's [7] method for finding the theoretical pressure drop through a channel with spacers is used to find theoretical values of $\Delta P_S$ for the triangular

and open-hexagonal lattices. Then a $\Delta P_S$ is found from experimental data gathered and correlated by de Stordeur[8] for triangular lattices. A ratio of experimental to theoretical spacer pressure drops is then obtained for triangular lattices. The theoretical pressure drop for the open-hexagonal lattice calculated from Tong's formulae are then multiplied by the ratio found above to obtain an appropriate semi-empirical spacer pressure loss for the open-hexagonal lattice. This approach thus uses the existing experimental data of de Stordeur to normalize the calculated results from Tong's method which is applicable, unlike de Stordeur's data, to both triangular and open-hexagonal lattices.

### 3.3 Theoretical Core and Spacer Pressure Drop

According to Tong "the pressure losses in a rod bundle due to the rod spacers are the form drag type pressure loss. This type of pressure drop can be calculated by using the pressure loss coefficients at sudden contraction, $K_c$, and at sudden expansion, $K_e$, as given by Kays and London[11]".[7] Values of $K_c$ and $K_e$ are reproduced in Fig. 3.1. The pressure losses at sudden contractions and expansions are given as follows:

For a sudden contraction

$$\Delta P_c = \frac{\rho V_2^2}{2g_c}(1-\sigma^2) + K_c\frac{\rho V_2^2}{2g_c} \quad \text{per spacer.} \qquad (3\text{-}1)$$

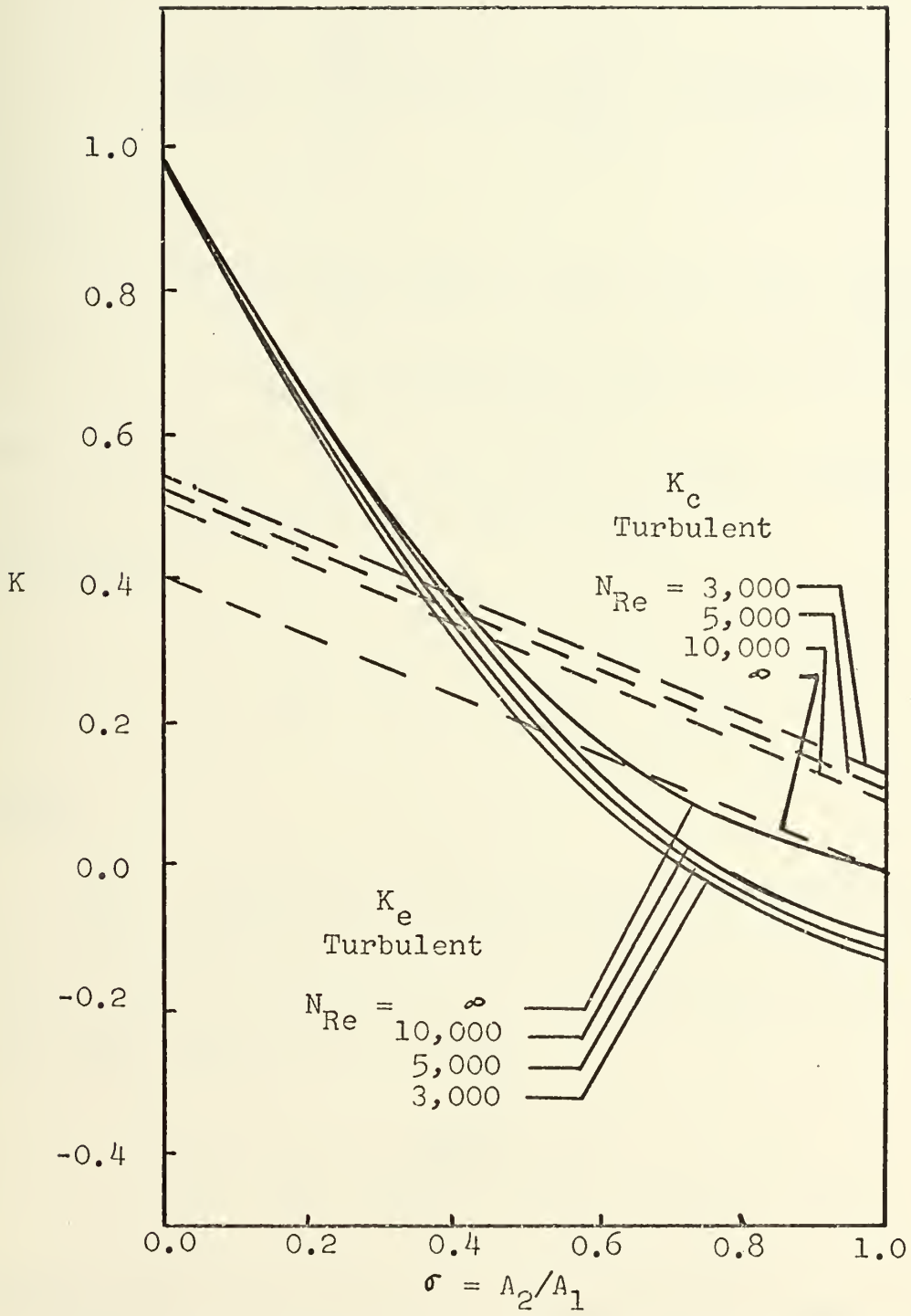


Fig. 3.1. Pressure loss coefficients at sudden contraction , $K_c$, and at sudden expansion, $K_e$, as given by Kays and London[9]. Taken from Ref. (7), Fig. 7.

For a sudden expansion

$$\Delta P_e = - \frac{\rho V_2^2}{2g_c}(1-\sigma^2) - K_e \frac{\rho V_2^2}{2g_c} \quad \text{per spacer,} \qquad (3\text{-}2)$$

where

$\sigma = A_2/A_1$ is the ratio of the flow in the gridded region to the flow area away from the gridded region,

$V_2$ is the velocity in the restricted cross-section region of the channel.

Note that positive $\Delta P$'s are pressure losses. Refer to Fig. 3.2 for definition of flow areas.

Therefore,

$$\Delta P_T - \Delta P_E = \Delta P_R \frac{f}{f_{cir}} + (\Delta P_S) \quad , \qquad (3\text{-}3)$$

where

$\frac{f}{f_{cir}}$ is the ratio of the friction factors in non-circular to circular channels; see Fig. 3.3[10].

Substituting an expression for the friction pressure drop in a duct into Eq. (3-3) gives

$$\Delta P_T - \Delta P_E = f_F \frac{4\rho l \bar{V}_1^2}{D_e 2g_c} \left(\frac{f}{f_{cir}}\right) + \Delta P_c + \Delta P_e \quad . \qquad (3\text{-}4)$$

Substituting expressions for $\Delta P_c$ and $\Delta P_e$ from Eqs. (3-1) and (3-2) into Eq. (3-4)

$$\Delta P_T - \Delta P_E = f_F \frac{4\rho l \bar{V}_1^2}{D_e 2g_c} \left(\frac{f}{f_{cir}}\right) + (K_c + K_e) \frac{\rho (A_1/A_2)^2 V_1^2}{2g_c} n_g \qquad (3\text{-}5)$$

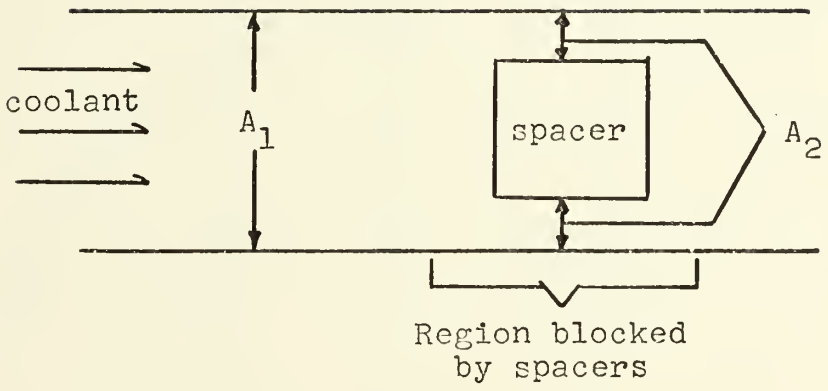


Fig. 3.2. Flow areas in a coolant cell. $A_1$ is the area away from the spacer region. $A_2$ is the free flow area in the spacer region.

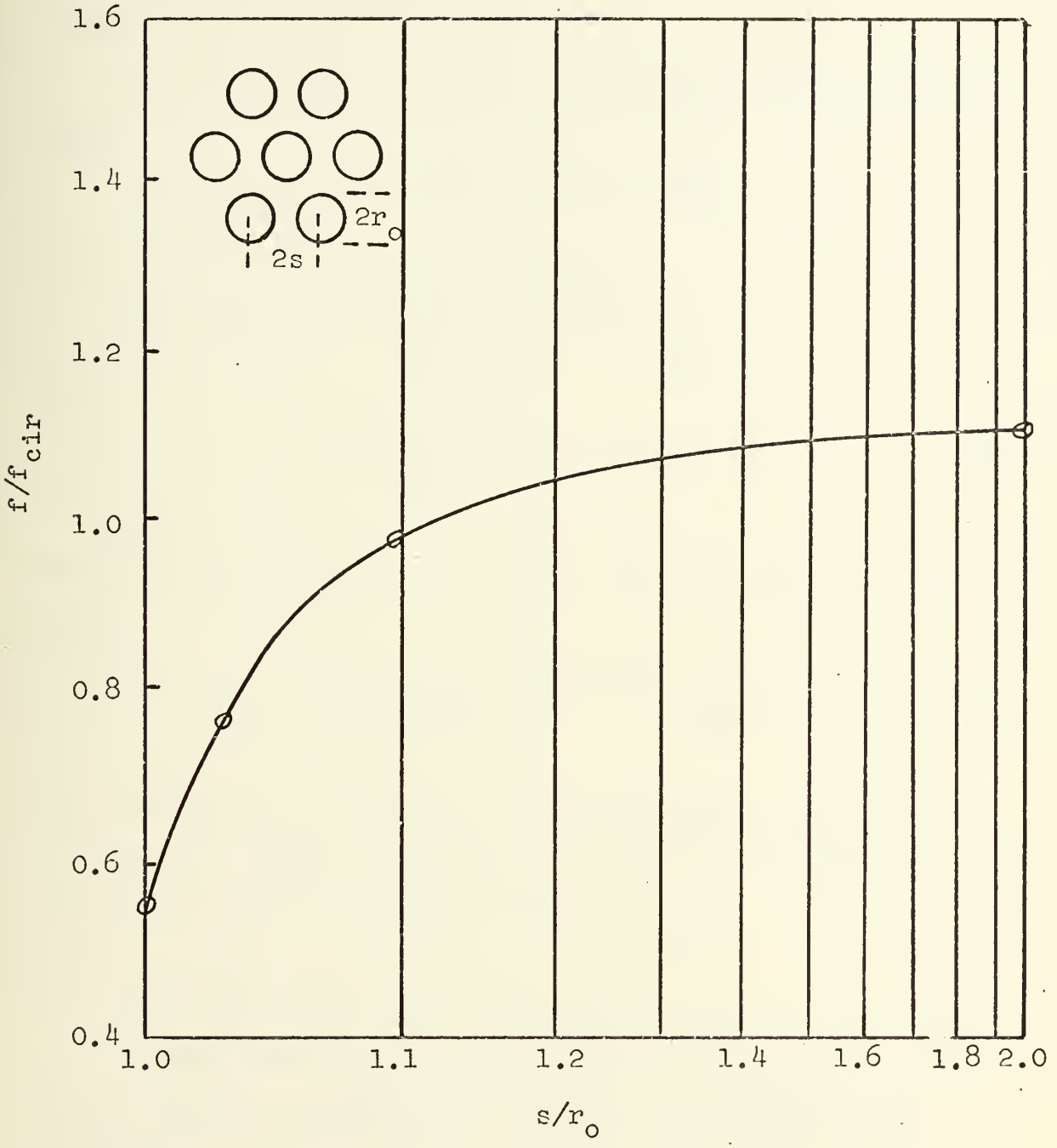


Fig. 3.3. Fully developed turbulent flow parallel to a bank of circular tubes of rods; points ⊙ based on friction coefficients calculated by Deissler and Taylor[11] at Re = $10^5$; Reynolds number influence is small, and Nusselt number behavior is virtually the same as friction behavior. Taken from Ref. (10), Fig. (9-10), which also shows that the ratio of Nusselt numbers is similar to the ratio of friction factors for non-metalic fluids.

where

$n_g$ is the number of spacer grid sets in the rod bundle.

Using

$$f_F = 0.046\ Re^{-0.2} \text{ for turbulent flow,}$$

Eq. (3-5) becomes

$$\Delta P_T - \Delta P_E = \frac{0.092\mu^{0.2}l\rho^{0.8}V_1^{1.8}}{D_e^{1.2}g_c}\left(\frac{f}{f_{cir}}\right) + \frac{\rho(A_1/A_2)^2V_1^2}{2g_c}(K_e + K_c)n_g \quad , \tag{3-6}$$

where $\bar{V}_1$ is found from $\bar{V} = \bar{\omega}/\rho A_1$ (ft/hr), and $\bar{\omega}$ is found from

$$\bar{\omega} = \left(\frac{g\beta\rho^2 Z_e D^{1.2}S^{1.8}\bar{q}_T}{0.092\mu^{0.2}Nc_p}\right)^{0.357} \quad \text{(lb/hr)} \quad . \tag{A-8}$$

The quantity $\bar{\omega}$ is the average mass flow rate for natural circulation derived in Appendix A, $n_r$ is the number of effective rods per cell and $\bar{q} = n_r\bar{q}'1$.

## 3.4 Empirical Spacer Pressure Drop

An empirical $\Delta P_S$ for a triangular lattice will now be found using de Stordeur's[8] method. According to de Stordeur

$$\Delta P_S = \frac{C_S V_S^2 S\rho}{2gA_1} \tag{3-7}$$

where

$C_S$ is the spacer drag coefficient

$V_S$ is the velocity in the spacer region (ft/sec)

$S$ is the spacer projected frontal area ($ft^2$)

$g$ is the gravitational acceleration ($ft/sec^2$)

$A_1$ is the flow area in the cell away from the gridded region ($ft^2$)

$\rho$ is the density of the coolant ($lb/ft^2$)

$\Delta P_S$ is the pressure loss due to one spacer ($lb/ft^2$)

Using appropriate values of $V_S$, $S$, $g$, $A_1$, $\rho$, and a $C_S$ taken from Fig. 3.4, an empirical spacer pressure drop, $\Delta P_S$, can be calculated from Eq. (3-7) for a triangular lattice with a honeycomb pin support grid.

We can now obtain the ratio of the empirical spacer pressure drop to the theoretical spacer pressure drop for a triangular lattice with a honeycomb grid and set it equal to the ratio of the empirical to theoretical spacer pressure drop for an open-hexagonal lattice:

$$\left[\frac{(\Delta P_S)_{em}}{(\Delta P_S)_{th}}\right]_t = \left[\frac{(\Delta P_S)_{em}}{(\Delta P_S)_{th}}\right]_h \quad . \tag{3-8}$$

An appropriate $(\Delta P_S)_{em}$ can be found from Eq. (3-8) for an open-hexagonal lattice after a $(\Delta P_S)_{th}$ for the open-hexagonal lattice has been calculated using Tong's method. Equation (3-6) then becomes

$$(\Delta P_T - \Delta P_E)_h = \frac{0.092\mu^{0.2}{}_1\rho^{0.8}V_1^{1.8}}{D_e^{1.2}g_c}\left(\frac{f}{f_{cir}}\right) +$$

$$\left(\frac{(\Delta P_S)_{em}}{(\Delta P_S)_{th}}\right)_t \frac{\rho(A_1/A_2)^2V_1^2}{2g_c}(K_e + K_c)n_g \quad . \tag{3-9}$$

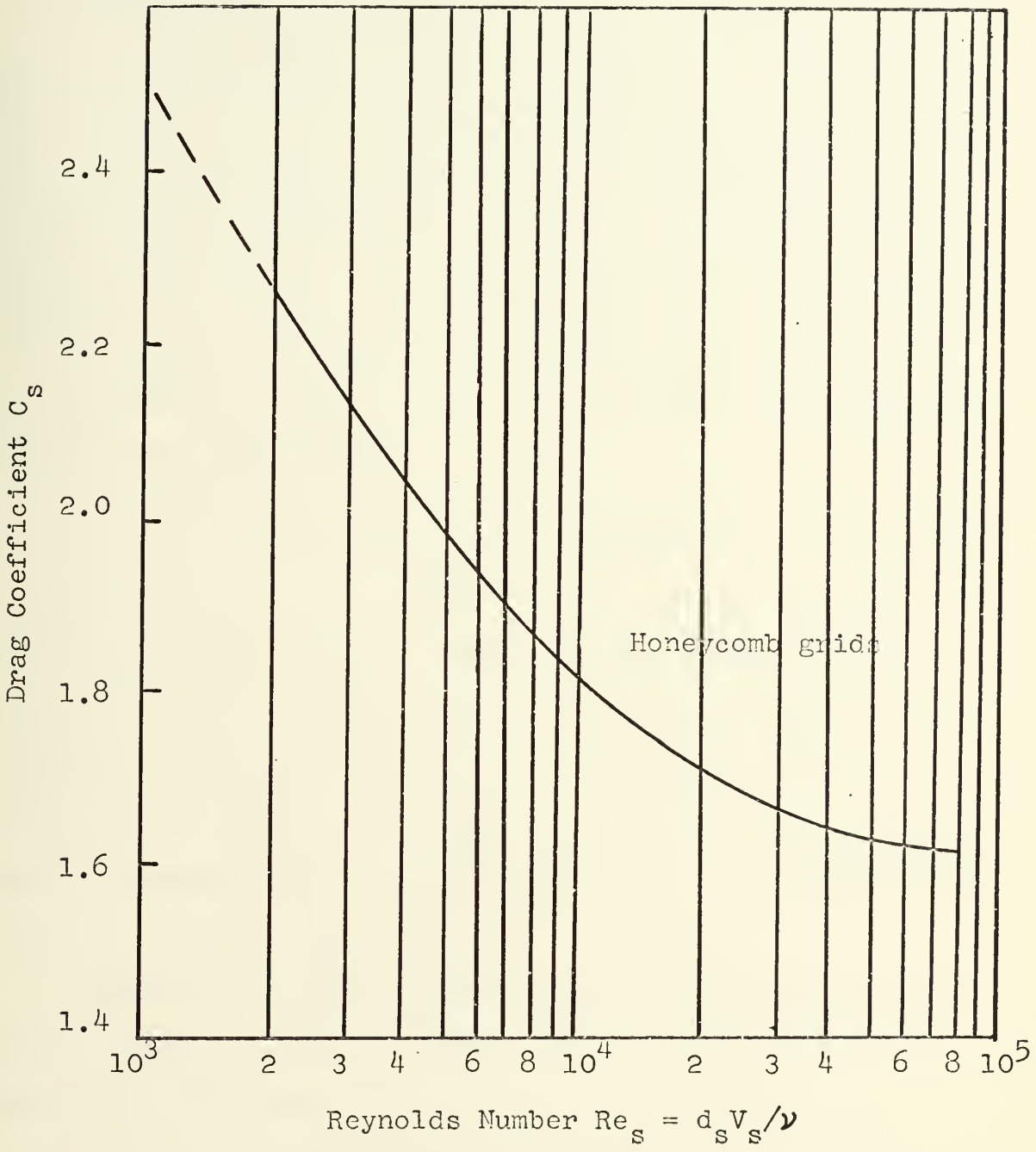


Fig. 3.4. Drag coefficients for honeycomb grid spacer. (Dashed line is an extrapolated portion of the curve.) The quantity $d_s$ is the spacer width.[8]

## 3.5 Mass Flow Rate and Linear Power in Steady-State Thermal Circulation

In steady-state thermal circulation the thermal buoyancy driving force, $\Delta P_B$, equals the friction pressure drop, $\Delta P_R$, for a pipe loop including the rod bundle section. See Appendix A for a derivation of mass flow rate and linear power relationships. For a rod bundle section the pressure losses through the spacers adds another component to the total pressure loss in the loop. The steady state pressure balance will then become

$$\Delta P_B = \Delta P_R \frac{f}{f_{cir}} + \Delta P_S = f_s \Delta P_R \quad , \qquad (3\text{-}10)$$

where $f_s$ is a multiplying ratio which accounts for spacer pressure drop. It is introduced in order to make the calculation of mass flow rates, pressure drops, and linear power output easier. The factor $f_s$ is found to be approximately constant for the range of velocities investigated in any given lattice configuration.

Substituting the relationships for $\Delta P_B$ from Eq. (A-3) and $\Delta P_R$ from Eq. (A-5) into Eq. (3-10) and solving for the mass flow rate gives

$$\bar{\omega} = \left(\frac{g\beta\rho^2 Z_e D^{1.2} S^{1.8} n_r \bar{q}'1}{0.092\mu^{0.2} N_c c_p f_s}\right)^{0.357} \quad , \qquad (3\text{-}11)$$

where $\bar{\omega}$ is the mass flow rate for a unit cell.

As shown in Eq. (A-3) the thermal buoyancy pressure gain

depends on the linear power and the mass flow rate, and the friction pressure drop depends on the mass flow rate. These dependencies can be seen in Fig. 3.5. In Fig. 3.5 Eq. (3-11) is the locus of points along the $\Delta P_R f_s$ line, and for any given $\bar{q}'_i$ the corresponding $\bar{\omega}$ can be taken from the graph. The dashed lines represent constant $t_h - t_c$ lines. Since

$$\bar{q}' = \frac{c_p \Delta t}{n_r l} \quad , \tag{3-12}$$

for any given core lattice geometry, any one of the three variables $\bar{q}'$, $\bar{\omega}$, $\Delta t$ can be found, given the other two. Solutions for a natural circulation operating condition will be the point of intersection of the three lines representing $\Delta P_s$ for a given $\bar{q}'$, $\Delta P_R f_s$, and $\Delta t$. Substituting Eq. (3-11) into Eq. (3-12)

$$\bar{q}' = \left(\frac{g\beta\rho^2 Z_e D_e^{1.2} S^{1.8} n_r}{0.092\mu^{0.2} N f_s}\right)^{0.555} \left(\frac{\Delta t}{n_r}\right)^{1.555} \left(\frac{c_p}{l}\right)^{1.0} \tag{3-13}$$

Equation (3-13) is the relationship for the intersection of the $\Delta P_R f_s$ line in Fig. 3.6 with a given $\Delta t$. The quantities $\bar{\omega}$ and $\Delta P_B$ are taken into account in Eq. (3-13).

## 3.6 Comparison of Linear Power Output in Open-hexagonal, Triangular, and Square Lattices

As shown in Fig. 1.2, the number of effective rods per cell for the three lattices is

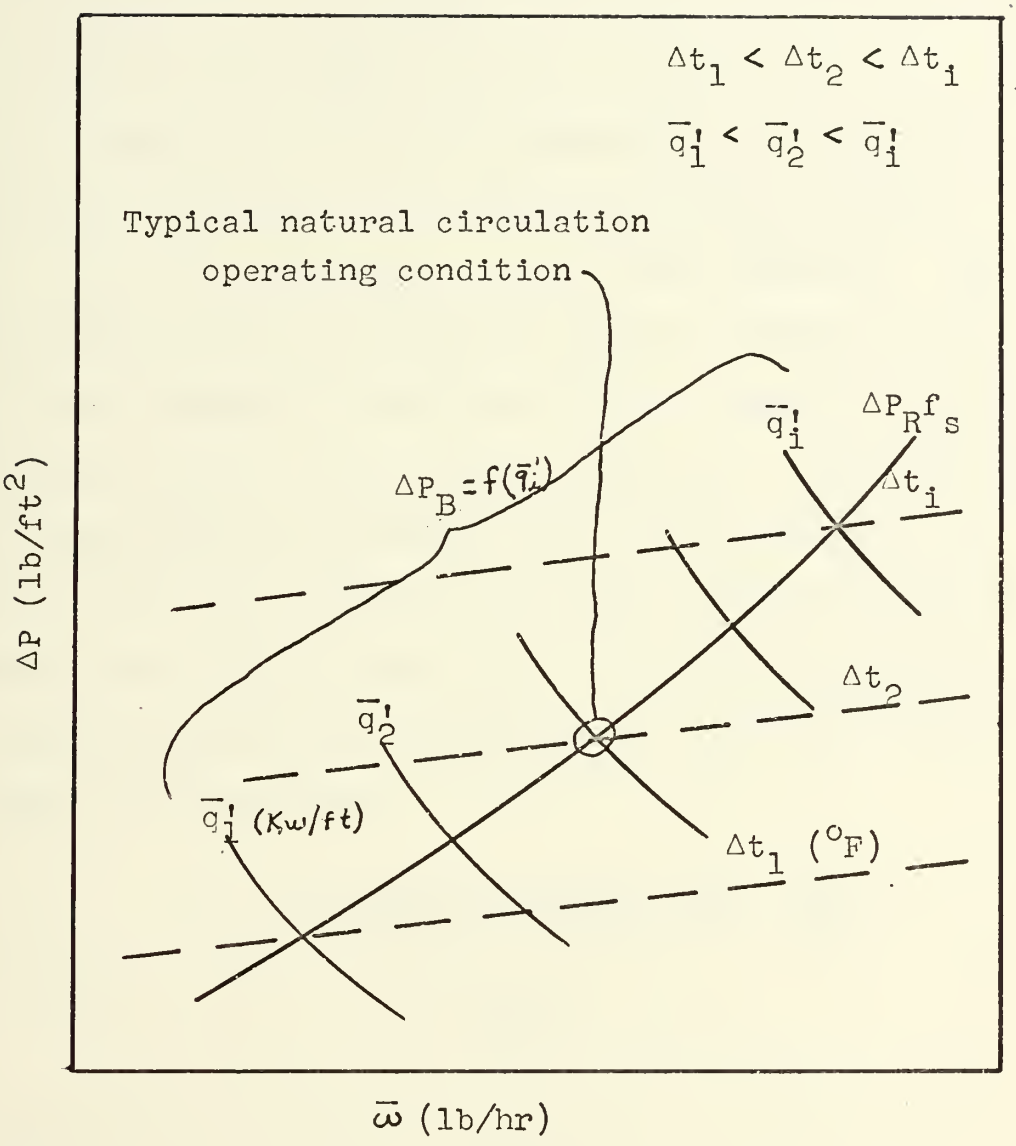


Fig. 3.5. Illustrative graph of solutions for natural circulation operating conditions. The intersection of the three lines defines an operating condition. The $\Delta P_R f_s$ line is defined by Eq. (A-6). $\Delta P_B$ lines are defined by Eq. (A-3). The $\Delta t$ lines are governed by Eq. (A-11).

open-hexagonal - $n_r = 2$

triangular - $n_r = 1/2$

square - $n_r = 1$

For this comparison it will be assumed for a first order approximation that the fluid properties of the coolant, $\Delta t$, $Z_e$, $f_s$, and $N_e$ are equal for the three lattices. The three lattices will be compared by taking a ratio of the linear power outputs of the three lattices based on equal fuel volume fraction and equal pin diameters. The variables will be the equivalent diameter, $D_e$, of a flow cell, the cross-sectional flow area, S, of a cell, and the number of effective fuel rods per cell, $n_r$. As shown in Appendix B, for equal $V_f'$ the hydraulic diameters of the three lattices are equal. By definition

$$D_e = \frac{4 \text{ x cross sectional area}}{\text{wetted perimeter}} = \frac{4S}{P_w} ,$$

or

$$S = \frac{P_w D_e}{4} .$$

Therefore,

$$S_h = \frac{\pi d D_e}{2} ,$$

$$S_t = \frac{\pi d D_e}{8} ,$$

$$S_{sq} = \frac{\pi d D_e}{4} .$$

Using Eq. (3-13) for $\bar{q}'$,

$$\bar{q}' = \left(\frac{g\beta\rho^2 z_e D_e^{1.2} S^{1.8} n_r}{0.092^{0.2} N_f}\right)^{0.555} \left(\frac{\Delta t}{n_r}\right)^{1.555} \left(\frac{c_p}{1}\right)^{1.0}, \quad (3\text{-}13)$$

we obtain the following ratios of linear power output:

$$\frac{\bar{q}'_h}{\bar{q}'_t} = \frac{(S^{1.8} n_r)_h^{0.555} (1/n_r)_h^{1.555}}{(S^{1.8} n_r)^{0.555} (1/n_r)_h^{1.555}}$$

$$= \frac{((\pi d D_e/2)^{1.8}(2))^{0.555} (1/2)^{1.555}}{((\pi d D_e/8)^{1.8}(1/2))^{0.555} (1/0.5)^{1.555}} \equiv 1$$

$$\frac{\bar{q}'_h}{\bar{q}'_{sq}} = \frac{((\pi d D_e/2)^{1.8}(2))^{0.555} (1/2)^{1.555}}{((\pi d D_e/4)^{1.8}(1))^{0.555} (1/1)^{1.555}} \equiv 1$$

$$\frac{\bar{q}'_{sq}}{\bar{q}'_t} \equiv 1$$

It is seen that the linear power output of the three lattices under natural circulation is the same for equal fuel volume fraction and equal pin diameters. This is a direct consequence of the fact that the hydraulic diameters are the same. It is also easily shown that power removal capabilities under forced convection laminar or turbulent flow conditions are also the same for the three lattices (see Appendix D).

In Chapter 4 some typical values of fluid and lattice

parameters will be used to calculate the pressure drops and mass flow rates for a range of linear power output. Using typical core and primary system parameter values, a $\bar{q}'$ for natural circulation will be calculated to see how this value compares to current linear power ratings for forced convection cooling.

# Chapter 4

## Example Calculations of Mass Flow Rate, Pressure Drop and Linear Power Output

### 4.1 Discussion

In Chapter 3 the relationships for the mass flow rate, the pressure drop, and the linear power output per cell were derived. In this chapter typical values for lattice parameters will be used to solve for the mass flow rate, the pressure drop, and linear power output for an open-hexagonal lattice and for a triangular lattice of equal fuel volume fraction, $V_f'$, and equal pin diameter. As was seen in Chapter 3, the linear power output for triangular, open-hexagonal and square lattice arrangements are equal for equal fuel volume fraction, for equal core temperature drop, and for equal fluid properties in the three lattices. This equality is based on the condition that the pressure drop through the flow cells of the three lattices is equal since coolant velocities are equal in the three lattices. This condition is not strictly accurate because of the differences in the spacer arrangements. These differences introduce only small second order errors and can be neglected in a first order calculation of the relative linear power output. However, since they cannot be neglected in more precise calculations of the mass flow rate and linear power output of any given lattice arrangement, we will include calculations of these effects and tables of values of mass

flow rates, velocities and core pressure drop for a range of linear power output from one to twenty kilowatts per foot for the different lattices.

## 4.2 Calculation of Flow Parameters and Theoretical Spacer Pressure Drop in the Open-hexagonal Flow Cell

Refer to Figs. 1.1.a and 1.2.a for definition of the parameters required to calculate the expression for the $V_f'$ of an open-hexagonal lattice. The values of the parameters used to calculate $(V_f')_h$ are $d_p = 0.300$ in., $\delta_h = 0.040$ in., and $p_h = 0.340$ in., from which

$$(V_f')_h = \frac{\pi\sqrt{3}}{9}\left(\frac{d_p}{p_h}\right)^2 = 0.472 \ . \qquad (4\text{-}1)$$

The value for $d_p$ is about as large a value as is being considered for present LMFBR's fueled with uranium dioxide. The value for $\delta_h$ is about as small a pin to pin spacing as is being considered.

The following values will be used in calculating mass flow rates, pressure drop, and linear power output for an open-hexagonal lattice flow cell:

$n_r$ = number of pins per cell = 2,

$A_p$ = cross sectional area of a fuel pin = $\pi d_p^2/4$ = 0.00049 $ft^2$,

$d_s$ = assumed spacer web thickness = 0.00125 ft,

$n_s$ = number of spacer segments per cell = 9

$l_s$ = length of one spacer segment = $p_h\sqrt{3}/3$ = 0.0164 ft,

$A_s$ = cross sectional area of spacers per cell = $n_s l_s d_s$
= 0.000184 $ft^2$,

$A_T$ = total cross sectional area of cell = $3\sqrt{3}p_h^2/2$
= 0.00209 $ft^2$,

$A_1$ = flow area away from the gridded region = $A_T - n_r A_p$
= 0.0011 $ft^2$,

$A_2$ = flow area in the gridded region = $A_1 - A_s$
=0.000918 $ft^2$ (see Fig. 3.2 for definition of flow regions),

$\sigma = A_2/A_1 = 0.834$.

Equation (3-11) can now be used to calculate the variation of flow rate with power output,

$$\bar{\omega} = \left(\frac{g\beta\rho^2 Z_e D_e^{1.2} S^{1.8} n_r \bar{q}'l}{0.092\mu^{0.2} N_e c_p f_s}\right)^{0.357}, \qquad (3\text{-}11)$$

with the following additional constants:

$g$ = 4.16 x $10^8$ $ft/hr^2$,

$\beta$ = 1.6 x $10^{-4}$ $^oF^{-1}$,

$\rho$ = 50 $lb/ft^3$,

$\mu$ = 0.5 lb/ft-hr,

$c_p$ = 0.3 BTU/lb-$^oF$,

$(Z_e/N_e)$ = 0.5,

$D_e$ = $(3\sqrt{3}p_h^2 - \pi d_p^2)/\pi d_p$ = 0.0281 ft,

$S$ = $A_1$ = 0.0011 $ft^2$,

$n_r$ = 2 rods,

$l$ = 4 ft,

$f_s$ = 1 (see Eq. (3-10) for a definition of $f_s$).

Thus, for example, for $\bar{q}' = 10$ kw/ft = 34130 BTU/hr-ft, the average mass flow rate for an open-hexagonal lattice flow cell is $\bar{\omega} = 602$ lb/hr. Table IV.1 lists values of mass flow rate, coolant velocity in the ungridded region of a flow cell and corresponding Reynolds number for the open-hexagonal lattice. The coolant flow is seen to be turbulent for the range of linear power output considered.

The following computations are sample calculations of the average coolant velocities in and away from the gridded region of an open-hexagonal flow cell for the $\bar{q}' = 10$ kw/ft case. These velocities will be used in finding the pressure drop due to the fuel pins and the spacers in the open-hexagonal flow cell. The quantity $\bar{V}_1$ is the average coolant velocity away from the gridded region:

$$(\bar{V}_1)_h = \bar{\omega}/\rho(A_1)_h = 10{,}966 \text{ ft/hr} .$$

The quantity $\bar{V}_2$ is the average coolant velocity in the gridded region:

$$(\bar{V}_2)_h = \bar{\omega}/\rho(A_2)_h = 13{,}164 \text{ ft/hr} .$$

The quantity $Re_1$ is the Reynolds number for the coolant away from the gridded region:

$$(Re_1)_h = D_e\rho(\bar{V}_1)_h/\mu = 30{,}815 .$$

The quantity $Re_2$ is the Reynolds number for the coolant in the gridded region:

Table IV.1

Flow Parameters for the Open-hexagonal Lattice

| $\bar{q}'$ (kw/ft) | $\bar{\omega}$ (lb/hr) | $\bar{V}_1$ (ft/hr) | $Re_1$ |
|---|---|---|---|
| 1 | 265 | 4,820 | 13,544 |
| 2 | 340 | 6,173 | 17,347 |
| 3 | 392 | 7,135 | 20,049 |
| 4 | 435 | 7,906 | 22,217 |
| 5 | 471 | 8,562 | 24,060 |
| 6 | 503 | 9,138 | 25,678 |
| 7 | 531 | 9,655 | 27,130 |
| 8 | 557 | 10,126 | 28,455 |
| 9 | 581 | 10,561 | 29,677 |
| 10 | 604 | 10,966 | 30,815 |
| 11 | 624 | 11,346 | 31,881 |
| 12 | 644 | 11,704 | 32,887 |
| 13 | 662 | 12,043 | 33,840 |
| 14 | 680 | 12,366 | 34,748 |
| 15 | 697 | 12,674 | 35,614 |
| 16 | 713 | 12,969 | 36,444 |
| 17 | 729 | 13,253 | 37,242 |
| 18 | 744 | 13,526 | 38,009 |
| 19 | 758 | 13,790 | 38,750 |
| 20 | 772 | 14,045 | 39,466 |

$$(Re_2)_h = D_e\rho(\bar{V}_2)_h/\mu = 36,990$$

From Fig. 3.3 for $\sigma = 0.834$, $K_c = 0.14$ and $K_e = -0.02$. Using Eqs. (3-3) and (3-6), the value for the total flow cell pressure drop is calculated:

$$(\Delta P_T - \Delta P_E) = \Delta P_R \frac{f}{Rf_{cir}} + \Delta P_s \qquad (3\text{-}3)$$

$$(\Delta P_T - \Delta P_E) = \frac{0.092\mu^{0.2}l\rho^{0.8}V_1^{1.8}}{D_e^{1.2}g_c}\left(\frac{f}{f_{cir}}\right) + \frac{\rho(A_1/A_2)^2V_1^2}{2g_c}(K_e + K_c)n_g \qquad (3\text{-}6)$$

$$(\Delta P_T - \Delta P_E)_h = 1.28 \times 10^{-6}V_1^{1.8}(1.02) + 0.052 \times 10^{-6}V_1^2$$

$$(\Delta P_T - \Delta P_E)_h = 30.7 \text{ lb/ft}^2 .$$

Table IV.2 lists values of $\Delta P_R$, $(\Delta P_R \frac{f}{Rf_{cir}})_h$, $((\Delta P_s)_{th})_h$, and $(\Delta P_T - \Delta P_E)_h$ for a range of linear power output. Since Reynolds numbers and velocities are equal for triangular and open-hexagonal lattices, $\Delta P_R$'s will be equal for the two lattices.

## 4.3 Calculations of Flow Parameters and Theoretical Spacer Pressure Drop in the Triangular Flow Cell

Refer to Figs. 1.1.b and 1.2.b for definition of the parameters required to calculate the expression for the $V_f'$

Table IV.2

Pressure Drop in the Open-hexagonal Lattice Flow Cell

| $\overline{V}_1$ (ft/hr) | $\Delta P_R$ (lb/ft$^2$) | $\Delta P_R f/f_{cir}$ (lb/ft$^2$) | $((\Delta P_s)_{th})_h$ (lb/ft$^2$) | $(\Delta P_T - \Delta P_E)_h$ (lb/ft$^2$) |
|---|---|---|---|---|
| 4,820 | 5.45 | 5.56 | 1.21 | 6.77 |
| 6,173 | 8.51 | 8.68 | 1.98 | 10.67 |
| 7,135 | 11.05 | 11.27 | 2.65 | 13.90 |
| 7,906 | 13.29 | 13.56 | 3.25 | 16.80 |
| 8,562 | 15.34 | 15.65 | 3.81 | 19.46 |
| 9,138 | 17.25 | 17.59 | 4.34 | 21.94 |
| 9,655 | 19.04 | 19.43 | 4.85 | 24.27 |
| 10,126 | 20.75 | 21.16 | 5.33 | 26.50 |
| 10,561 | 22.38 | 22.83 | 5.80 | 28.63 |
| 10,966 | 23.95 | 24.43 | 6.25 | 30.68 |
| 11,346 | 25.46 | 25.97 | 6.69 | 32.67 |
| 11,704 | 26.93 | 27.47 | 7.12 | 34.59 |
| 12,043 | 28.35 | 28.92 | 7.54 | 36.46 |
| 12,366 | 29.73 | 30.33 | 7.95 | 38.28 |
| 12,674 | 31.08 | 31.70 | 8.35 | 40.05 |
| 12,969 | 32.39 | 33.04 | 8.75 | 41.79 |
| 13,253 | 33.68 | 34.35 | 9.13 | 43.49 |
| 13,526 | 34.94 | 35.64 | 9.51 | 45.15 |
| 13,790 | 36.18 | 36.90 | 9.89 | 46.79 |
| 14,045 | 37.39 | 38.14 | 10.26 | 48.39 |

of a triangular lattice. Using the same fuel volume fraction and fuel pin diameter as were used for the open-hexagonal lattice,

$$(V_f')_t = \frac{\pi}{2\sqrt{3}}\left(\frac{d_p}{p_t}\right)^2 = 0.472 \ . \qquad (4\text{-}2)$$

Solving for the pitch and the pin to pin spacing gives:

$p_t = 0.416$ in.

$\delta_t = 0.116$ in.

The following values will be used in calculating mass flow rates, pressure drop, and linear power output for a triangular lattice flow cell:

$n_r = 1/2$,

$A_p = 0.00049$ ft$^2$,

$d_s = 0.00125$ ft,

$n_s = 1.5$,

$l_s = 0.02$ ft,

$A_s = 0.0000375$ ft$^2$,

$A_T = \sqrt{3}p_t^2/4 = 0.00052$ ft$^2$,

$A_1 = 0.000275$ ft$^2$,

$A_2 = 0.000237$ ft$^2$ (see Fig. 3.2 for definition of flow regions),

$\sigma = A_2/A_1 = 0.865$.

Equation (3-11) can again be used together with the following additional constants:

$g = 4.16 \times 10^8$ ft/hr$^2$,

$\beta = 1.6 \times 10^{-4}$ $^oF^{-1}$,

$\rho$ = 50 lb/ft$^3$,

$\mu$ = 0.5 lb/ft-hr,

$c_p$ = 0.3 BTU/lb-$^oF$,

$(Z_e/N_e)$ = 0.5,

$D_e$ = $(2\sqrt{3}p_t^2 - \pi d_p^2)/\pi d_p$ = 0.0281 ft,

$S$ = $A_1$ = 0.000274 ft$^2$,

$n_r$ = 1/2,

$l$ = 4 ft,

$f_s$ = 1.

Thus, for example, for $\bar{q}'$ = 10 kw/ft = 34130 BTU/hr-ft, the average mass flow rate for a triangular lattice flow cell is $\bar{\omega}$ = 150.5 lb/hr.

Table IV.3 lists values of mass flow rate, coolant velocity away from the gridded region, and the corresponding Reynolds number for the triangular lattice. Note that the corresponding coolant velocities and Reynolds numbers are the same for the open-hexagonal lattice since the fuel volume fractions are equal. Note also that the mass flow rates for the triangular lattice flow cell are one fourth of the corresponding mass flow rates for an open-hexagonal lattice flow cell. The differences are due to the differences in flow area, $A_1$, per cell and in the number of effective fuel rods, $n_r$, per cell. The mass flow rates per unit flow area, $\bar{\omega}/A_{cell}$, are equal for the two lattices.

The following computations are sample calculations of the average coolant velocities in and away from the gridded

Table IV.3

Flow Parameters for the Triangular Lattice

| $\bar{q}'$ (kw/ft) | $\bar{\omega}$ (lb/hr) | $\bar{V}_1$ (ft/hr) | $Re_1$ |
|---|---|---|---|
| 1 | 66 | 4,820 | 13,544 |
| 2 | 85 | 6,173 | 17,347 |
| 3 | 98 | 7,135 | 20,049 |
| 4 | 108 | 7,906 | 22,217 |
| 5 | 118 | 8,562 | 24,060 |
| 6 | 125 | 9,138 | 25,678 |
| 7 | 132 | 9,655 | 27,130 |
| 8 | 139 | 10,126 | 28,455 |
| 9 | 145 | 10,561 | 29,677 |
| 10 | 150 | 10,966 | 30,815 |
| 11 | 155 | 11,346 | 31,881 |
| 12 | 161 | 11,704 | 32,887 |
| 13 | 165 | 12,043 | 33,840 |
| 14 | 170 | 12,366 | 34,748 |
| 15 | 174 | 12,674 | 35,614 |
| 16 | 178 | 12,969 | 36,444 |
| 17 | 182 | 13,253 | 37,242 |
| 18 | 186 | 13,526 | 38,009 |
| 19 | 189 | 13,790 | 38,750 |
| 20 | 193 | 14,045 | 39,466 |

region of a triangular flow cell for the $\bar{q}' = 10$ kw/ft case. These velocities will be used in finding the pressure drop due to the fuel pins and the spacers in the triangular lattice flow cell. The procedure is the same as that used in finding the pressure drop in the open-hexagonal lattice flow cell in Section 4.2.

$$(\bar{V}_1)_t = \bar{\omega}/\rho(A_1)_t = 10{,}966 \text{ ft/hr},$$

$$(\bar{V}_2)_t = \bar{\omega}/\rho(A_2)_t = 12{,}701 \text{ ft/hr}.$$

Note that $(\bar{V}_1)_t = (\bar{V}_1)_h$ since the fuel volume fractions are equal, but $(\bar{V}_2)_t$ is slightly less than $(\bar{V}_2)_h$ since the grid configurations are different for the two lattices.

$$(Re_1)_t = D_e\rho(\bar{V}_1)_t/\mu = 30{,}815$$

$$(Re_2)_t = D_e\rho(\bar{V}_2)_t/\mu = 35{,}688$$

From Fig. 3.3 for $\sigma = 0.865$, $K_c = 0.12$ and $K_e = -0.03$. Again using Eqs. (3-3) and (3-6), the value for the total flow cell pressure drop is calculated:

$$(\Delta P_T - \Delta P_E)_t = 1.28 \times 10^{-6}\bar{V}_1^{1.8}(1.095) + 0.036 \times 10^{-6}\bar{V}_1^2 ,$$

$$(\Delta P_T - \Delta P_E)_t = 30.54 \text{ lb/ft}^2 .$$

The lattice pressure drop $(\Delta P_T - \Delta P_E)_h$ and $(\Delta P_T - \Delta P_E)_t$ are very close in value. This is due to the offsetting effects of the values of the $f/f_{cir}$ factors and the values

of the spacer pressure drop on the values of $(\Delta P_T - \Delta P_E)$ of the two lattices. Table IV.4 lists values of $\Delta P_R$, $(\Delta P_{Rf}\frac{f}{f_{cir}})_t$, $((\Delta P_s)_{th})_t$, and $(\Delta P_T - \Delta P_E)$ for a range of linear power outputs.

## 4.4 Empirical Spacer Pressure Drop for the Triangular and Open-hexagonal Lattices

The method of de Stordeur for finding the empirical spacer pressure drop in a triangular lattice was presented in Section 3.4. Inserting the following values into Eq. (3-7), here repeated, and solving for $((\Delta P_s)_{em})_t$,

$$\Delta P_s = \frac{C_s V_s^2 S \rho}{2 g A_1}, \qquad (3\text{-}7)$$

$g = 4.16 \times 10^8$ ft/hr$^2$,

$A_1 = 0.000274$ ft$^2$,

$V_s = \bar{V}_2 = 12{,}687$ ft/hr,

$S = A_s = 0.0000375$ ft$^2$,

$\rho = 50$ lb/ft$^3$,

$C_s = 2.33$ (see Fig. 3.4 where $Re_s = d_s V_s \rho/\mu = 1{,}586$),

gives

$$((\Delta P_s)_{em})_t = 3.08 \text{ lb/ft}^2\text{-grid}.$$

Using the theoretical spacer pressure drop calculated for a triangular lattice in Section 4.3:

$$((\Delta P_s)_{th})_t = \frac{4.34 \text{ lb/ft}^2}{5 \text{ grids}} = 0.868 \text{ lb/ft}^2\text{-grid}.$$

Table IV.4

Pressure Drop in the Triangular Lattice Flow Cell

| $\bar{V}_1$ (ft/hr) | $\Delta P_R$ (lb/ft$^2$) | $\Delta P_R f/f_{cir}$ (lb/ft$^2$) | $((\Delta P_s)_{th})_t$ (lb/ft$^2$) | $(\Delta P_T - \Delta P_E)_t$ (lb/ft$^2$) |
|---|---|---|---|---|
| 4,820 | 5.45 | 5.97 | 0.84 | 6.80 |
| 6,173 | 8.51 | 9.32 | 1.37 | 10.69 |
| 7,135 | 11.05 | 12.10 | 1.84 | 13.93 |
| 7,906 | 13.29 | 14.55 | 2.25 | 16.80 |
| 8,562 | 15.34 | 16.80 | 2.64 | 19.44 |
| 9,138 | 17.25 | 18.89 | 3.00 | 21.90 |
| 9,655 | 19.04 | 20.85 | 3.36 | 24.20 |
| 10,126 | 20.75 | 22.72 | 3.69 | 26.41 |
| 10,561 | 22.38 | 24.51 | 4.02 | 28.52 |
| 10,966 | 23.95 | 26.23 | 4.34 | 30.57 |
| 11,346 | 25.46 | 27.88 | 4.64 | 32.51 |
| 11,704 | 26.93 | 29.49 | 4.93 | 34.42 |
| 12,043 | 28.35 | 31.04 | 5.22 | 36.26 |
| 12,366 | 29.73 | 32.55 | 5.50 | 38.06 |
| 12,674 | 31.08 | 34.03 | 5.78 | 39.81 |
| 12,969 | 32.39 | 35.47 | 6.06 | 41.53 |
| 13,253 | 33.68 | 36.88 | 6.32 | 43.20 |
| 13,526 | 34.94 | 38.26 | 6.58 | 44.84 |
| 13,790 | 36.18 | 39.62 | 6.84 | 46.46 |
| 14,045 | 37.39 | 40.94 | 7.10 | 48.04 |

Therefore,

$$((\Delta P_s)_{em})_h = \left(\frac{(\Delta P_s)_{em}}{(\Delta P_s)_{th}}\right)_t ((\Delta P_s)_{th})_h = 3.56((\Delta P_s)_{th})_h \ .$$

The pressure drop for the open-hexagonal lattice is

$$(\Delta P_T - \Delta P_E)_h = \frac{0.092\mu^{0.2}{}_1\rho^{0.8}\overline{V}_1^{1.8}}{D_e^{1.2}g_c}\left(\frac{f}{f_{cir}}\right)$$

$$+ \left(\frac{(\Delta P_s)_{em}}{(\Delta P_s)_{th}}\right)_t \frac{\rho(A_1/A_2)^2\overline{V}_1^2}{2g_c}(K_e + K_c)n_g \ ,$$

$$(\Delta P_T - \Delta P_E)_h = 24.4 + 3.59(6.25) = 46.8 \text{ lb/ft}^2.$$

Calculating the factor, $f_s$, gives (see Eq. (3-10)):

$$(f_s)_h = \frac{\Delta P_R f/f_{cir} + (\Delta P_s)_{em}}{\Delta P_R} = 1.96 \ .$$

Table IV.5 lists values of $V_s$, $Re_s$, $C_s$, $((\Delta P_s)_{em})_t$, $((\Delta P_s)_{th})_t$, $((\Delta P_s)_{em}/(\Delta P_s)_{th})_t$, and $((\Delta P_s)_{em})_h$ used in finding $(f_s)_h$ for a range of linear power output from one to twenty kilowatts per foot. $(\Delta P_R)_h$ and $(\Delta P_R f/f_{cir})_h$ are found in Table IV.2. The factor $(f_s)_h$ is relatively constant, with an average value of 1.95. The quantity $(\Delta P_T - \Delta P_E)_h = (\Delta P_R f_s)_h$ is also tabulated in Table IV.5.

For more accurate pressure drop calculations, $(f_s)_h$ should be used in Eq. (A-8) for finding the mass flow rate

Table IV.5

Flow Parameters and Pressure Drop in the Spacer Region for the Triangular Lattice Flow Cell

| $\bar{q}'$ (kw/ft) | $V_s$ (ft/hr) | $Re_s$ --- | $C_s$ --- | $((\Delta P_s)_{em})_t$ lb/ft$^2$-grid |
|---|---|---|---|---|
| 1 | 5,577 | 697 | 2.68 | 0.68 |
| 2 | 7,142 | 893 | 2.56 | 1.07 |
| 3 | 8,255 | 1,032 | 2.51 | 1.41 |
| 4 | 9,147 | 1,143 | 2.47 | 1.70 |
| 5 | 9,906 | 1,238 | 2.44 | 1.97 |
| 6 | 10,573 | 1,322 | 2.41 | 2.21 |
| 7 | 11,171 | 1,396 | 2.39 | 2.45 |
| 8 | 11,716 | 1,464 | 2.38 | 2.69 |
| 9 | 12,219 | 1,527 | 2.36 | 2.90 |
| 10 | 12,687 | 1,586 | 2.35 | 3.11 |
| 11 | 13,127 | 1,641 | 2.34 | 3.31 |
| 12 | 13,542 | 1,693 | 2.33 | 3.51 |
| 13 | 13,934 | 1,742 | 2.32 | 3.70 |
| 14 | 14,307 | 1,788 | 2.31 | 3.89 |
| 15 | 14,664 | 1,833 | 2.30 | 4.07 |
| 16 | 15,005 | 1,876 | 2.29 | 4.24 |
| 17 | 15,334 | 1,917 | 2.28 | 4.41 |
| 18 | 15,650 | 1,956 | 2.27 | 4.57 |
| 19 | 15,955 | 1,994 | 2.26 | 4.73 |
| 20 | 16,250 | 2,031 | 2.25 | 4.91 |

Table IV.5 continued

| $((\Delta P_s)_{th})_t$ (lb/ft$^2$) | $\left(\frac{(\Delta P_s)_{em}}{(\Delta P_s)_{th}}\right)_t$ | $((\Delta P_s)_{em})_h$ lb/ft$^2$-grid | $(f_s)_h$ --- | $(\Delta P_R f_s)_h$ (lb/ft$^2$) |
|---|---|---|---|---|
| 0.84 | 4.10 | 4.96 | 1.93 | 10.63 |
| 1.37 | 3.92 | 7.76 | 1.93 | 16.59 |
| 1.84 | 3.83 | 10.15 | 1.94 | 21.55 |
| 2.25 | 3.78 | 12.27 | 1.94 | 25.92 |
| 2.64 | 3.73 | 14.20 | 1.95 | 29.90 |
| 3.00 | 3.68 | 15.99 | 1.95 | 33.64 |
| 3.36 | 3.65 | 17.72 | 1.95 | 37.13 |
| 3.69 | 3.64 | 19.39 | 1.95 | 40.46 |
| 4.02 | 3.61 | 20.92 | 1.95 | 43.64 |
| 4.34 | 3.59 | 22.44 | 1.96 | 46.70 |
| 4.64 | 3.58 | 23.92 | 1.96 | 49.65 |
| 4.93 | 3.56 | 25.36 | 1.96 | 52.51 |
| 5.22 | 3.55 | 26.74 | 1.96 | 55.28 |
| 5.50 | 3.53 | 28.07 | 1.96 | 57.97 |
| 5.78 | 3.51 | 29.34 | 1.96 | 60.60 |
| 6.06 | 3.59 | 30.62 | 1.97 | 63.16 |
| 6.32 | 3.48 | 31.80 | 1.96 | 65.68 |
| 6.58 | 3.47 | 33.00 | 1.96 | 68.13 |
| 6.84 | 3.45 | 34.16 | 1.96 | 70.55 |
| 7.10 | 3.45 | 35.44 | 1.97 | 72.91 |

of the open-hexagonal lattice flow cell. Coolant velocities and cell and spacer pressure drop would be recomputed to find a corrected $(f_s)_h$. This process would be continued until succeeding $(f_s)_h$'s were essentially constant.

The factor, $f_s$, for the triangular lattice is calculated by the same procedure as was used to calculate $(f_s)_h$. The average value of $(f_s)_t$ is 1.74. The factor, $(f_s)_t$, is not equal to $(f_s)_h$ since the spacer pressure drop in the two lattices are different, a condition due to the difference in spacer configuration in the two lattices.

4.5 Linear Power Output for the Open-hexagonal Lattice

Using Eq. (3-13),

$$\bar{q}' = \left(\frac{g\beta\rho^2 Z_e D_e^{1.2} S^{1.8} n_r}{0.092\mu^{0.2} N_e f_s}\right)^{0.555} \left(\frac{\Delta t}{n_r}\right)^{1.555} \left(\frac{c_p}{l}\right)^{1.0}, \qquad (3\text{-}13)$$

the average linear power for the open-hexagonal lattice is calculated using the following constants:

$g = 4.16 \times 10^8$ ft/hr$^2$,

$\beta = 1.6 \times 10^{-4}$ $^\circ$F$^{-1}$,

$\rho = 50$ lb/ft$^3$,

$\mu = 0.5$ lb/ft-hr,

$c_p = 0.3$ BTU/lb/$^\circ$F,

1 kw = 3413 BTU/hr .

In terms of several system variables, the linear power output can be expressed as

$$\bar{q}' = 22.4\left(\left(\frac{Z_e}{N_e}\right)^{0.555}\left(\frac{1}{f_s}\right)^{0.555}\left(\frac{\Delta t}{100}\right)^{1.555} D_e^{0.666}\left(\frac{S}{n_r l}\right)^{1.0}\right) , \quad (4\text{-}3)$$

where $\Delta t$ is in $^{\circ}F$, $D_e$ is in inches, S is in square inches, and l is in feet. Inserting the following typical values into Eq. (4-3):

$Z_e/N_e$ = 0.5 (i. e., the ratio of the source/sink elevation difference and the effective primary circuit length),

$\Delta t$ = 400 $^{\circ}F$,

S = 0.1587 $in.^2$ (the cross sectional flow area for the open-hexagonal flow cell in these calculations),

$f_s$ = 1.95,

$D_e$ = 0.337 in. (the equivalent diameter for the open-hexagonal flow cell in these calculations),

$n_r$ = 2 rods,

l = 4 ft,

the average linear power output for the open-hexagonal lattice (and for the triangular and square lattices) is

$$\bar{q}'_h = 0.873 \text{ kw/ft} .$$

The above value for $\bar{q}'$ is low compared to the required full power output of a practical reactor, which averages around 10 kw/ft. On the other hand, 8.73% of full power is a respectable rating in terms of decay heat removal. Suggestions for increasing the value of the linear power output achievable with natural circulation flow are made in Chapter 6.

The mass flow rates, $\bar{\omega}$, coolant velocities, $\bar{V}$, and friction pressure drop, $\Delta P_R$, calculated in the preceding example were based on an $f_s = 1$. Table IV.6 lists the mass flow rates per unit flow area, $\bar{\omega}/A_{cell}$, and the total friction pressure drop, $\Delta P_R f_s$, calculated using $(f_s)_h = 1.95$ and $(f_s)_t = 1.74$ in Eq. (3-11). The tube bundle friction pressure drop, $\Delta P_R$, was calculated from

$$\Delta P_R = 1.28 \times 10^{-6} \bar{V}_1^{1.8} \text{ lb/ft}^2 ,$$

where

$$\bar{V}_1 = \frac{\bar{\omega}}{\rho A_1} .$$

Figure 4.1 shows the natural circulation operating conditions for the open-hexagonal and triangular lattices. Using a $\Delta t = 400\ ^{\circ}F$, the linear power output of the two lattices vary by the factor $(1/f_s)^{0.357}$. Since $(A_{cell})_h = 4(A_{cell})_t$ and $\bar{\omega}_h \approx 4\bar{\omega}_t$, the horizontal axis of Fig. 4.1 is in units of $\bar{\omega}/A_{cell}$ for ease of comparison of the performance of the two lattices. Figure 4.1, which is based on the values in Table IV.6, shows that for equal total friction pressure drop and equal $\Delta t$, the triangular lattice has a slightly higher linear power output than does the open-hexagonal lattice.

Table IV.6

Mass Flow Rates per Unit Flow Area and Total Friction Pressure Drop as Functions of a Calculated $f_s$ in the Open-hexagonal and Triangular Flow Cells

| $\bar{q}'$ (kw/ft) | $(\bar{\omega}/A_{cell})_h$ (lb/hr-ft$^2$) | $(\Delta P_R f_s)_h$ (lb/ft$^2$) | $(\bar{\omega}/A_{cell})_t$ (lb/hr-ft$^2$) | $(\Delta P_R f_s)_t$ (lb/ft$^2$) |
|---|---|---|---|---|
| 1 | 190,000 | 6.9 | 198,000 | 6.6 |
| 2 | 243,500 | 10.8 | 253,500 | 10.4 |
| 3 | 281,000 | 14.0 | 292,500 | 13.5 |
| 4 | 311,500 | 16.8 | 324,500 | 16.2 |
| 5 | 337,500 | 19.4 | 351,500 | 18.7 |
| 6 | 360,500 | 21.8 | 375,000 | 21.1 |
| 7 | 380,500 | 24.1 | 396,000 | 23.2 |
| 8 | 399,000 | 26.3 | 415,500 | 25.3 |
| 9 | 416,000 | 28.4 | 433,500 | 27.3 |
| 10 | 432,500 | 30.4 | 450,500 | 29.2 |

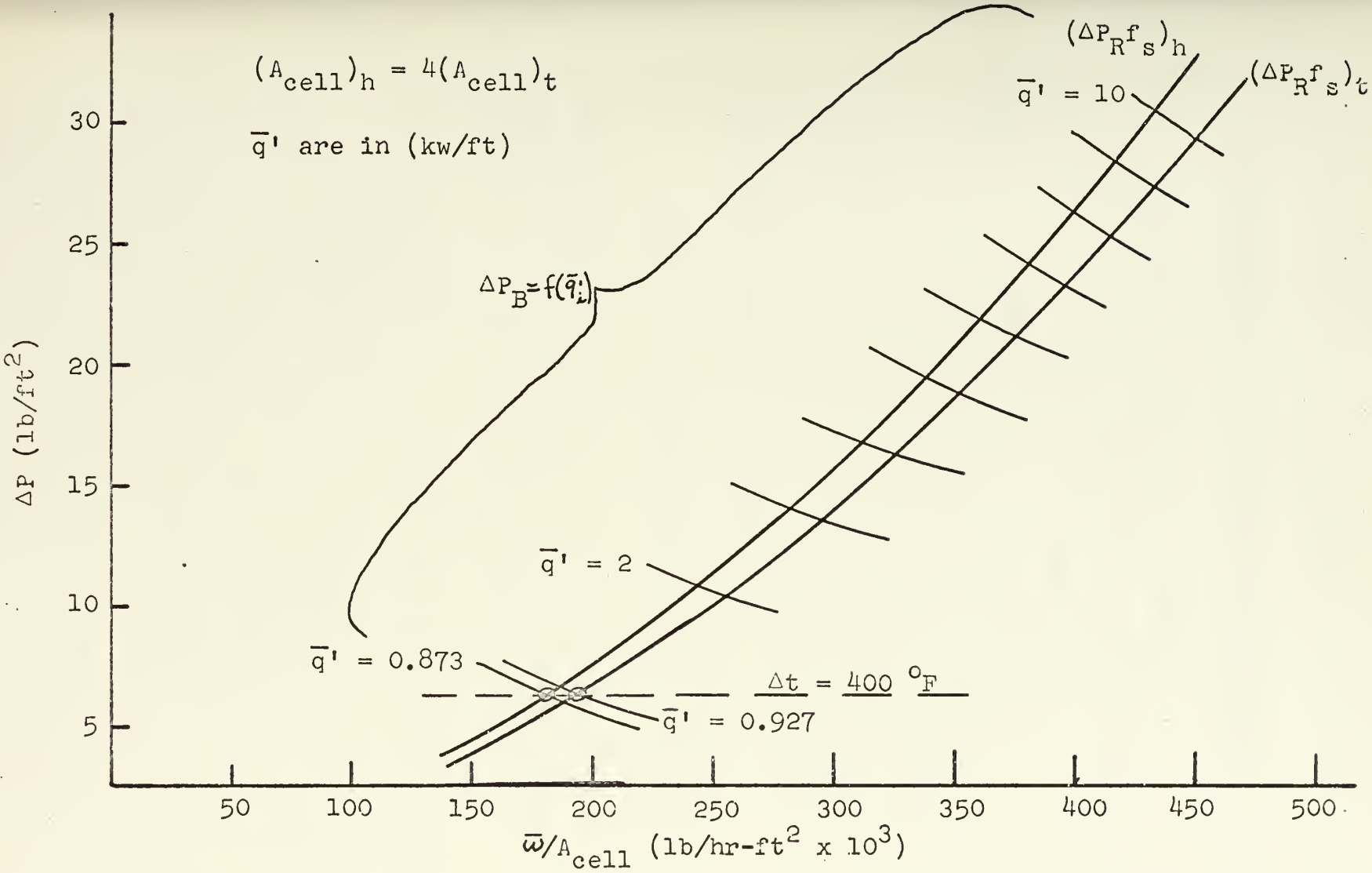


Fig. 4.1. Natural circulation operating conditions denoted by ⊙ for the open-hexagonal and triangular lattices.

# Chapter 5

## Equivalent Diameter for the Open-hexagonal Lattice

### 5.1 Definition of Equivalent Diameter

Whenever flow in noncircular ducts is considered, it is necessary to employ in the calculation of the Reynolds number and friction factor some characteristic dimension. In circular ducts the characteristic dimension is the diameter, D. In noncircular ducts the concept of equivalent diameter, $D_e$, (also referred to as hydraulic diameter) applies when the duct does not appreciably vary from circular. The equivalent diameter is defined as

$$D_e = \frac{4 \times \text{cross sectional flow area}}{\text{wetted perimeter}} = \frac{4A}{P_w} \quad . \qquad (5\text{-}1)$$

The equivalent diameter is the characteristic length which would give the same ratio of fluid passage volume to wetted area for circular and noncircular ducts.

### 5.2 Conditions for a Laminar Flow Region in the Open-hexagonal Flow Cell

In a noncircular duct the concept of equivalent diameter applies for turbulent or laminar flow. However, the values for the Reynolds number and friction factor are different for laminar and turbulent flow. In a unit open-hexagonal cell (refer to Fig. 1.2.a) the flow passage is approximately circular; therefore, the concept of equivalent

diameter should apply. In Chapter 4 the Reynolds number and friction factor for the open-hexagonal cell were calculated assuming fully turbulent flow in all parts of the cell. These numbers were computed using the average cell rate of flow which was turbulent. For turbulent flow

$$f_F = 0.046 Re^{-0.2} \quad .$$

However, it is possible that the flow is laminar in some sections of the flow cell, namely, in the narrow flow area between two adjacent fuel pins. If this is the case, then the Reynolds number and friction factor are different in the laminar flow area from the Reynolds number and friction factor in the rest of the flow area. For laminar flow

$$f_F = 16 Re^{-1} \quad .$$

In order to determine if the flow in the region between adjacent fuel pins is fully laminar, a rough calculation of the laminar sub-layer thickness around the fuel pins will be made. The pin to pin spacing is 0.040 inches; therefore, if the laminar sub-layer around each pin is as much as 0.020 inches, the region may be considered to have laminar flow. If this be the case, the open-hexagonal flow cell can be divided into two channels, one having turbulent flow and one having laminar flow. This division of the flow cell assumes no inter-channel mixing and little or no heat transfer from the laminar region to the turbulent region. This

assumption is not good if there is a significant degree of inter-channel coolant mixing, which in fact probably occurs in the present case since the channels are not isolated. This assumption breaks down also if the heat transfer from channel to channel is good.

If it is found that open-hexagonal cells can be divided into two channels, the coolant flow rates would have to be recomputed using two flow regions per cell in order that the power output could be recomputed. Since the pressure drop through the subassembly, $\Delta P_{SA}$, will be the same for all flow regions, the coolant velocity in the laminar channel will be less than the coolant velocity in the turbulent channel in accordance with:

$$(\Delta P_{SA})_{Lam} = (\Delta P_{SA})_{Tur} \quad ,$$

$$(4f\frac{L\rho V^2}{D_e 2})_{Lam} = (4f\frac{L\rho V^2}{D_e 2})_{Tur} \quad .$$

From this last relation it follows that

$$V_{Lam} < V_{Tur} \quad , \qquad (5\text{-}2)$$

since the friction factor for fully laminar flow is greater than the friction factor for fully turbulent flow in a smooth pipe or duct, and the laminar region $D_e$ is approximately less than or equal to the turbulent region $D_e$. Calculations of the equivalent diameters for the two regions showed $(D_e)_{Lam} \leq (D_e)_{Tur}$ in the open-hexagonal flow cell.

Since $V_{Lam} < V_{Tur}$, then $\omega_{Lam} < \omega_{Tur}$, where $\omega_{Lam}$ is the mass flow rate in the laminar channel of the flow cell, and $\omega_{Tur}$ is the mass flow rate in the turbulent channel of the flow cell. If it is desired to maintain the core $\Delta t$ at a certain amount, then $(\omega_{Lam} + \omega_{Tur}) < \omega_{sr}$ where $\omega_{sr}$ is the flow rate based on a single region of fully turbulent flow in the entire flow cell. The sum of $\omega_{Lam}$ and $\omega_{Tur}$ is less than $\omega_{sr}$ because $\omega_{Lam}$ in the laminar channel is less than $\omega_{Tur}$. Since $c_p$ and $\Delta t$ are constant and $(\omega_{Lam} + \omega_{Tur}) < \omega_{sr}$, then $\bar{q}_{Tot}$ will have to be decreased from the value calculated in a single region (turbulent) flow correlation $(\bar{q}_{Tot})_{sr} = \omega_{sr} c_p \Delta t$, thus degrading the power output of the entire core.

## 5.3 Calculation of Laminar Sub-layer Thickness in Turbulent Flow

The thickness of the laminar sub-layer around the fuel pins will be calculated to a first order approximation using equations given by Schlichting[12]. The laminar momentum sub-layer thickness, $\delta_l$, for turbulent flow in pipes is given by Schlichting's Eq. (20.15a) as

$$\delta_l \approx \frac{\nu}{\bar{v}_*} \quad . \tag{5-3}$$

The friction velocity, $v_*$, is given by his Eq. (20.8) as

$$v_* = (T_o/\rho)^{1/2} = (0.03955 \bar{\mu}^{-7/4} \nu^{1/4} d^{-1/4})^{1/2} \quad , \tag{5-4}$$

where

$T_o$ is the shear stress at the wall,

$\bar{u}$ is the average velocity in the pipe,

$\nu$ is the kinematic fiscosity of the fluid,

d is the pipe diameter.

Using the following values from the example calculations in Chapter 4:

$d = (D_e)_h = 0.0281$ ft

$\bar{u} = \bar{V}_1 = 10{,}966$ ft/hr

$\nu = \mu/\rho = 0.01$ ft$^2$/hr

the friction velocity is $v_* = 598$ ft/hr, and the laminar momentum sub-layer thickness $\delta_1 \approx 0.001$ in. The thermal boundary layer thickness on the other hand is $\delta_{th} \approx k/h$. Using the following approximate values for liquid sodium:

$k = 40$ BTU/hr-ft-°F,

$h = 20{,}000$ BTU/hr-ft$^2$-°F,

the thermal boundary layer is $\delta_{th} \approx 0.002$ in.

These values of $\delta_1$ and $\delta_{th}$ are considerably less than 0.020 inches, the value necessary to establish a laminar flow region between adjacent fuel pins. Therefore, the flow in all regions of the open-hexagonal flow cell can be considered to have turbulent flow. Consequently, the open-hexagonal flow cell can be considered to have only one flow region, and an equivalent diameter, defined by Eq. (5-1), can be calculated for the entire cell.

The above calculations of $\delta_1$ and $\delta_{th}$ were only approximate. A more accurate computer calculation using a code

such as General Electric's Velvet-II Code[13] can be made of the velocity profiles around the fuel pins. However, there is no reason to expect that more sophisticated calculations would alter the above conclusions.

# Chapter 6

## Summary and Conclusions

### 6.1 Summary

The work reported in the preceding chapters has compared the open-hexagonal, triangular, and square lattice configurations under natural circulation flow with respect to leakage reactivity effects in a coolant cell upon sodium voiding, mass flow rate and pressure drop in the coolant channels, and linear power output. The basis for comparison of the three lattices was equal fuel rod size and volumetric composition in the cores. The open-hexagonal lattice was found to be preferable from the standpoint of leakage reactivity upon sodium voiding because of its larger coolant channel nuclear hydraulic radius. For the same cell bulk temperature rise the mass flow rates per cell flow area, $\bar{\omega}_{cell}/A_{cell}$, were found to be equal for the three lattice flow cells. The pressure drop through the lattices were approximately equal; the small differences in pressure drop were due to the differences in spacer configuration. The linear power outputs of the three lattices were found to be equal for the three lattices assuming equal core pressure drop. Example calculations of the above quantities were presented. It was also found that the fluid flow and heat transfer characteristics of the three lattices were equal under forced circulation for both laminar and turbulent flow. Finally, the applicability of the equivalent diameter

concept for use in calculation of heat transfer and fluid flow characteristics of the open-hexagonal flow cell was examined. It was found that the conventional expression for equivalent diameter can be used for the open-hexagonal lattice.

## 6.2 Discussion

The open-hexagonal lattice was found to be superior to the triangular and square lattices with respect to leakage reactivity upon sodium voiding. If more sophisticated calculations confirm that the added negative leakage component of the sodium void reactivity effect in the open-hexagonal lattice is indeed several dollars, there would be a definite advantage from a safety standpoint in employing this lattice in either natural or forced convection LMFBR's.

However, from the standpoint of hydraulic and thermal performance examined in this study, the open-hexagonal lattice was not found to be superior to the triangular or square lattices in any way. The triangular lattice would, in fact, be preferable to an open-hexagonal lattice since more fuel pins can be packed into a given area of core while still maintaining prudent pin to pin spacings. Assuming the present FFTF pin spacing of 0.0625 inches for a triangular lattice and equal pin diameters of $d_p$ = 0.300 inches for both lattices, the fuel pins in the open-hexagonal lattice would have to be touching per Eq. (B-1) in order to retain an equal fuel volume fraction in the two lattices. If a pin to pin spacing for the open-hexagonal lattice were to be held at 0.040 inches, the $V_f$ as calculated in Appendix C

would have to be held to around 0.306 without considering stainless steel swelling and to 0.288 with consideration given to stainless steel swelling. Larger pin sizes for the open-hexagonal lattice would allow larger $V_f$, but the increase in $V_f$ would not be significant if the pin to pin spacing was held at a reasonable value ($\delta_h < 0.020$ inches). This can be seen from the decreasing slope of the $V_f'$ versus $d_p$ curve of Fig. C.1. Current and future design values for $V_f$ are found in Table C.1.

Since the natural convection performance of all three lattices is equal in the hydraulic and thermal aspects examined, improvements in the linear power output achieved by all three lattices can be suggested using Eq. (A-10),

$$\bar{q}' = \left(\frac{g\beta\rho^2 Z_e D_e^{1.2} S^{1.8} n_r}{0.092\mu^{0.2} N_e f_s}\right)^{0.555} \left(\frac{\Delta t}{n_r}\right)^{1.555} \left(\frac{c_p}{l}\right)^{1.0}. \qquad \text{(A-10)}$$

In Chapter 4 a value for $Z_e/N_e$, the ratio of the source/sink elevation difference and the effective primary circuit length, of 0.5 was employed. This ratio can be increased. Using values from the FFTF design proposals for a 400 Mwt LMFBR[14], a typical value for $N_e$ is

$$N_e = \frac{\Delta P_{pump}}{\Delta P_{core}} L_{core} = 11.6 \text{ ft},$$

where

$$\Delta P_{pump} = 145 \text{ psi}$$

$\Delta P_{core}$ = 100 psi

$L_{core}$ = 8 ft

By employing a $Z_e$ of up to say 24 feet, the ratio $Z_e/N_e$ could be made as large as 2.0. For a value of $Z_e/N_e = 2.0$, the linear power output calculated in Chapter 4 would be increased by a factor of $(2.0/0.5)^{0.555} = 2.16$. In Chapter 4 the value of the core temperature rise was 400 °F. If this value could be raised to 450 °F, the linear power output would be increased by a factor of $(450/400)^{1.555} = 1.2$. A core $\Delta t$ of 400 °F is about as large a value as is practical. A larger value of $\Delta t$ may produce a thermal shock upon reactor scram which the primary system could not withstand. The linear power output could also be increased by spacing the fuel pins farther apart while increasing pin diameter. The wider spacing would increase the equivalent diameter, $D_e$, and coolant flow area, S, thus increasing $\overline{q}'$ since $\overline{q}' = f((D_e^{1.2}S^{1.8})^{0.555}) = f(D_e^{0.666}S)$. The core temperature rise, $\Delta t$, would also increase with this change in spacing through the relation $\overline{q}'\eta_r l = \overline{q} = \overline{\omega} c_p \Delta t$. However, the spacing contribution probably would not increase $\overline{q}'$ by much. In Chapter 4 the core length, l, was four feet. The length l could possibly be reduced by as much as two feet, thus raising $\overline{q}'$ by the factor $(4/2)^{1.0} = 2$. Combining the above suggested contributions for increasing $\overline{q}'$ gives a total factor of about 5.2. With these contributions $\overline{q}'$ would equal 4.54 kw/ft instead of 0.873 kw/ft as calculated

in Chapter 4. However, 4.54 kw/ft is in reality a peak value for the natural circulation case. It is less than 50% of the desired 10 kw/ft average and less than 30% of the 16 kw/ft peak (assuming axial and radial peaking factors of about 1.25 and 1.26) needed to match projected 1000 Mwe forced convection plant operating conditions[15A]. Unless a better combination of the variables discussed above can be achieved, full power operation under natural circulation is not practical.

A summary of the parameters assumed and calculated in this study is presented in Table VI.1.

## 6.3 Future Work

Since the leakage reactivity effect in the open-hexagonal lattice provides a significant additional negative reactivity contribution compared to the triangular and square lattices, a more sophisticated calculation by Monte Carlo or other methods should be made to determine a precise value for the sodium void negative reactivity component in the open-hexagonal lattice. The model used in this study yielded only approximate answers under the assumption of an infinite core. An experiment measuring the relative and absolute negative reactivity of the lattices should also be considered. However, since the reactivity change is on the order of one percent of the effective multiplication factor, the necessary precision for measuring the reactivity change would be difficult to design into the experiment.

Table VI.1

Assumed and Calculated Core Parameters for Various Lattices

| Item | Units | Source | Triangular | Open-hexagonal | Square |
|---|---|---|---|---|---|
| $V_f'$ | $ft^3/ft^3$ | App. C, Chap. 4 | 0.472 assumed | 0.472 assumed | 0.472 assumed |
| d | in. | App. C, Chap. 4 | 0.300 assumed | 0.300 assumed | 0.300 assumed |
| $\delta$ | in. | App. C | 0.116 | 0.040 assumed | ---- |
| p | in. | App. C | 0.416 | 0.340 | ---- |
| $n_r$ | rods | Fig. 1.1 | 1/2 | 2 | 1 |
| $D_e$ | ft | App. B, Chap. 4 | 0.0281 | 0.0281 | 0.0281 |
| $S = A_1$ | $ft^2$ | Eqs. (D-4)-(D-6) | $A_h/4$ | $A_h$ =0.0011 | $A_h/2$ |
| $\bar{\omega} \propto (n_r S^{1.8})^{0.357}$ | lb/hr | App. A, Chap. 4 | $\bar{\omega}_h/4$ | $\bar{\omega}_h$ = 602 | ---- |
| $\bar{\omega}/A_{cell}$ | $\frac{lb/hr}{ft^2}$ | Chap. 4 | 547,000 | 547,000 | 547,000 |
| $V=\frac{\bar{\omega}}{\rho S} \propto (\frac{n_r}{S})^{0.357}$ | ft/hr | Chap. 4 | 10,966 | 10,966 | 10,966 |
| $\Delta P_R = 4f \frac{L \rho V^2}{F D_e 2 g_c}$ | $lb/ft^2$ | Chap. 4 | 23.95 | 23.95 | 23.95 |
| $f_s$ | $\frac{lb/ft^2}{lb/ft^2}$ | Eq. (3-10) | 1.74 | 1.95 | ---- |

Models of the three lattices could be constructed to test the pressure drop performance of the different configurations. Freon or water could be used as the test coolant.

## 6.4 Conclusion

This study has shown that from hydraulic and thermal aspects, the triangular, open-hexagonal and square lattices are essentially equivalent under forced and natural circulation. For natural circulation operation it was shown that the linear power output of the three lattices was far less than the desired value for full power operation, even under an optimum combination of constraints. Therefore, nome of the lattices are practical for full power operation under natural circulation. Furthermore, unless the open-hexagonal lattice is found to contribute significantly to the negative component of the sodium void reactivity effect, the triangular lattice is preferable for forced convection operation.

## Appendix A

### Linear Power Relationship for Natural Circulation in a Reactor

If z is the elevation above a datum surface (see Fig. A.1) at which the pressure is constant, the difference in pressure between elevations $z_2$ and $z_1$ in a static fluid (no friction nor acceleration) is

$$P_2 - P_1 = \int_{z_2}^{z_1} \frac{\rho g dz}{g_c} = \frac{\bar{\rho} g (z_1 - z_2)}{g_c} . \qquad (A\text{-}1)$$

Integrating completely around a closed circuit which has the fluid in two legs at different densities gives

$$\Delta P_B = \frac{g}{g_c}\left(\int_{z_2}^{z_1} \rho_c dz + \int_{z_1}^{z_2} \rho_h dz\right),$$

$$\Delta P_B = \frac{g}{g_c} \int_{z_1}^{z_2} (\rho_h - \rho_c) dz .$$

Introducing the temperature coefficient of volumetric expansion, $\beta$:

$$\rho_h - \rho_c = \rho_c \beta_c (t_h - t_c) ,$$

$$\Delta P_B = \frac{g \rho_c \beta_c}{g_c} \int_{z_i}^{z_2} (t_h - t_c) dz . \qquad (A\text{-}2)$$

Using $\bar{q} = \bar{\omega} c_p (t_h - t_h)$ where $\bar{q}$ is the heat produced per

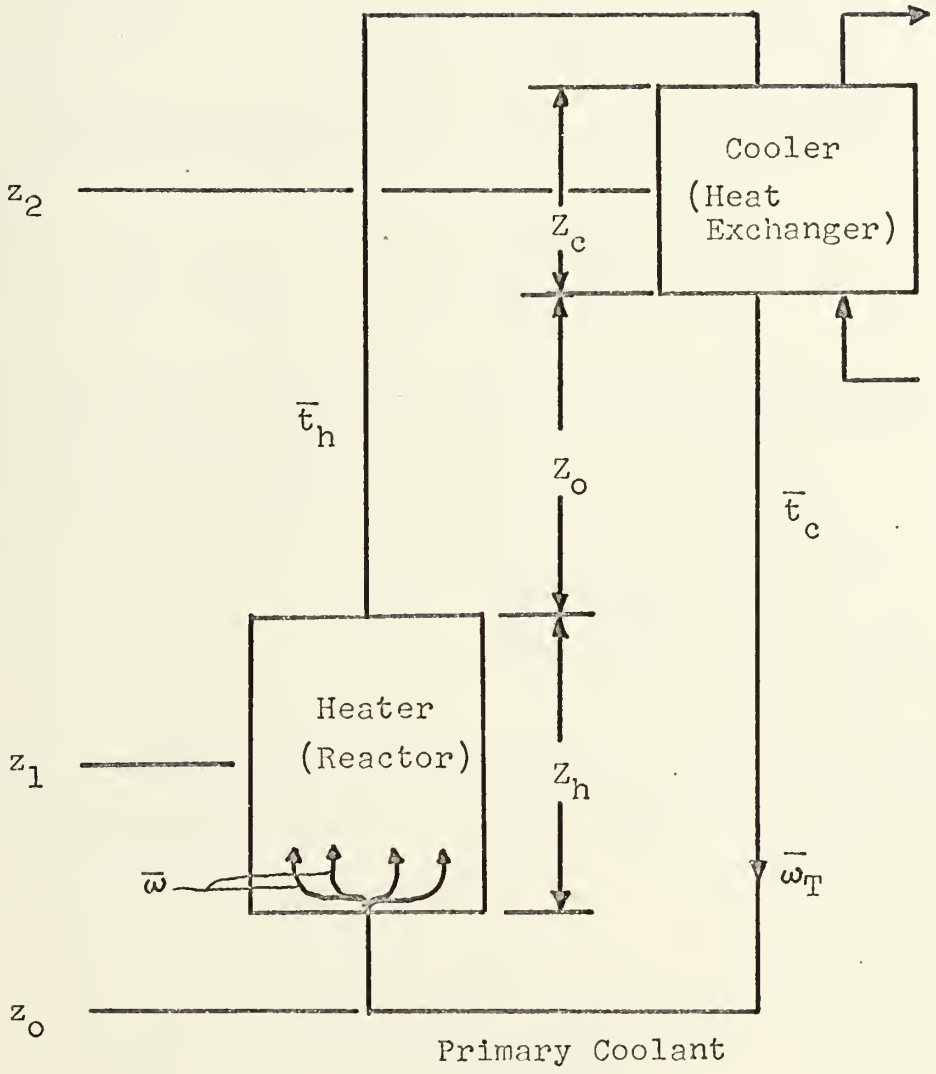


Fig. A.1. Thermal circulation driving heads.(16)

unit cell, and $\bar{\omega}$ is the mass flow rate per cell and $z_2 - z_1 = Z_e = Z_0 + (Z_c + Z_h)/2$,

$$\Delta P_B = \frac{g\beta_c \rho_c \bar{q} Z_e}{g_c c_p \bar{\omega}} \quad . \tag{A-3}$$

From the definition of the Fanning friction factor,

$$f_F = \frac{\Delta P_R g_c D}{2N_e \rho \bar{\omega}^2} \quad , \tag{A-4}$$

an expression for the friction pressure drop, $\Delta P_R$, is obtained as follows:

$$\Delta P_R = \frac{2N_e \rho \bar{\omega}^2 f_F f_s}{g_c D_e \rho^2 S^2} \quad , \tag{A-5}$$

where $f_s$, the factor accounting for spacer pressure drop, is defined by Eq. (3-10), and $\bar{u} = \bar{\omega}/\rho S$. Equating $\Delta P_B$ and $\Delta P_R$ and solving for $\bar{\omega}$ gives

$$\bar{\omega} = \left(\frac{g\beta\rho^2 \bar{q} Z_e D_e S^2}{2N_e c_p f_F f_s}\right)^{1/3} \quad . \tag{A-6}$$

In this derivation $N_e$ is the total effective length of the primary coolant system:

$$N_e = \frac{\Delta P_{pump} L_{core}}{\Delta P_{core}}$$

where $L_{core}$ is the length of the core. The quantity $N_e$ is a measure of the equivalent length of the complete primary circuit (core, pipes, and heat exchanger) expressed in terms of an extended core of height $N_e$ and channel diameter $D_e$. Substituting the relationship $f_F = 0.046Re^{-0.2}$ $= 0.046\mu^{0.2}/(D_e\bar{\omega}/S)^{0.2}$ for turbulent flow into Eq. (A-6) gives

$$\bar{\omega} = \left(\frac{g\beta\rho^2 Z_e D_e^{1.2} S^{1.8} \bar{q}}{0.092\mu^{0.2} N_e c_p f_s}\right)^{0.357} . \qquad \text{(A-7)}$$

Using the relationships $\bar{q} = n_r \bar{q}' l$, where $n_r$ is the number of effective fuel rods per unit cell, and $\bar{q} = \bar{\omega} c_p \Delta t$, where $\Delta t = t_h - t_c$:

$$q' = \frac{\bar{\omega} c_p \Delta t}{n_r l} . \qquad \text{(A-8)}$$

Substituting Eq. (A-7) into Eq. (A-8) yields

$$\bar{q}' = \left(\frac{g\beta\rho^2 Z_e D_e^{1.2} S^{1.8} n_r \bar{q}' l}{0.092\mu^{0.2} N_e c_p f_s}\right)^{0.357} \left(\frac{c_p \Delta t}{n_r l}\right) . \qquad \text{(A-9)}$$

Solving for $\bar{q}'$, Eq. (A-9) becomes

$$\bar{q}' = \left(\frac{g\beta\rho^2 Z_e D_e^{1.2} S^{1.8} n_r}{0.092\mu^{0.2} N_e f_s}\right)^{0.555} \left(\frac{\Delta t}{n_r}\right)^{1.555} \left(\frac{c_p}{l}\right)^{1.0} . \qquad \text{(A-10)}$$

Refer to Fig. 3.6, which is reproduced below as Fig. A.2, for the physical illustration of these results. Fig. A.3 shows a comparison of the driving forces in the forced and natural convection cases.

For natural convection the following observations are made: If it is desired to increase $\bar{q}'$, this is done by allowing an increase in $\Delta t$. This in effect increases the driving head allowing a greater flow rate, $\bar{\omega}$ per Eq. (A-8) at which the $\Delta P_B = \Delta P_R$. The combination of an increase in both $\Delta t$ and $\bar{\omega}$ increases $\bar{q}$ according to the relation $\bar{q} = \bar{\omega} c_p (t_h - t_c)$, and thereby $\bar{q}'$ increases for fixed $n_r$ and $l$, since $\bar{q}' = \bar{q}/n_r l$.

Note if $\Delta t$ is fixed, i. e., a maximum allowable core temperature drop is specified, the cell operating condition for constant cell parameters $n_r$ and $l$ is fixed at the intersection of the three lines $\Delta t$, $\Delta P_R$, and $\Delta P_B$. This intersection fixes $\bar{\omega}$ and hence $\bar{q}$ and $\bar{q}'$ through $\bar{q} = \bar{\omega}_{fixed} c_p (t_h - t_c)_{fixed}$ and $\bar{q}' = \bar{q}/n_r l = \bar{\omega} c_p \Delta t / n_r l$ from Eq. (A-10).

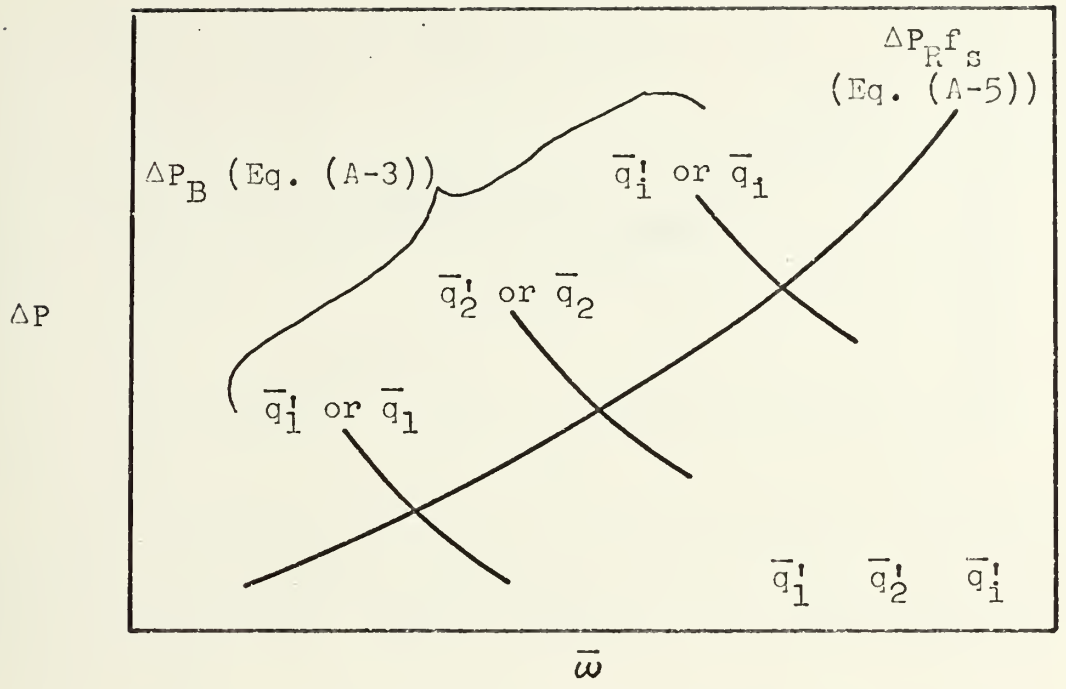


a. Intersection points given by Eq. (A-7).

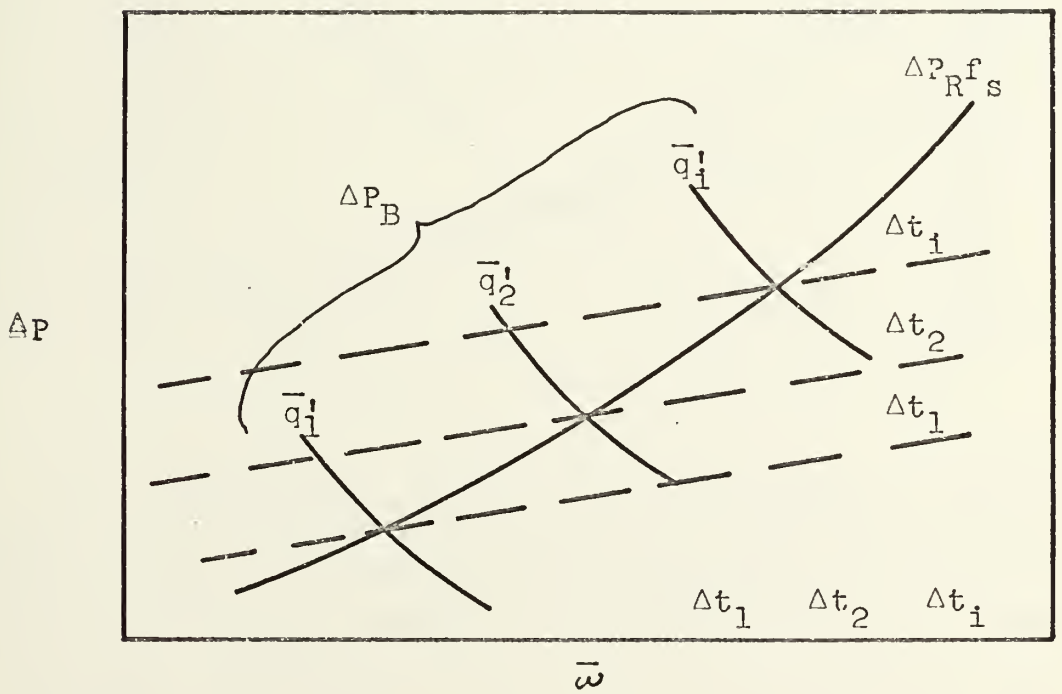


b. Eq. (A-10) yields the $\bar{q}'$ which corresponds to the intersection points of the three lines; i. e., for conditions of $\Delta P_B = \Delta P_R$ and $\Delta t$ fixed.

Fig. A.2. Natural circulation operating conditions.

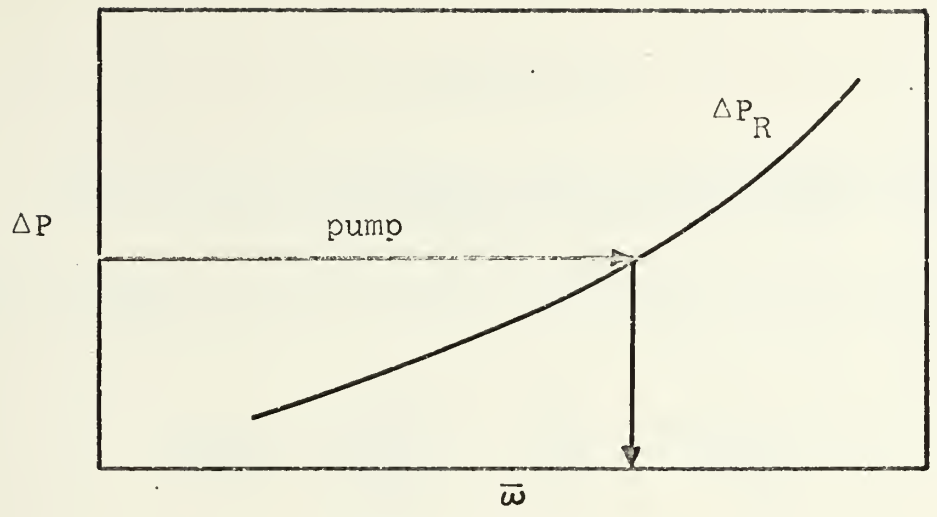


a. Relationship between driving pressure and mass flow rate in a forced convection system where, for a fixed $\Delta t$, $\bar{q}' = \bar{\omega} c_p \Delta t / n_r l$, and $\bar{\omega}$ depends on the pump pressure.

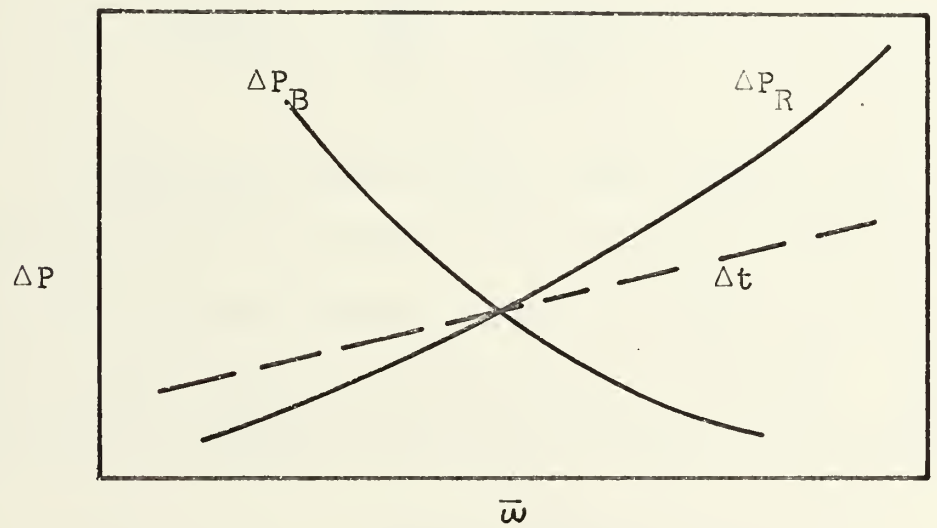


b. Relationships between driving pressure, mass flow rate, and core temperature rise in a natural convection system where, for a fixed $\Delta t$, $\bar{q}' = \bar{\omega} c_p \Delta t / n_r l$ is found by Eq. (A-10), and $\bar{\omega}$ is determined as the intersections of lines of $\Delta t$, $\Delta P_B$, and $\Delta P_R$.

Fig. A.3. Comparison of driving forces in forced and natural convection.

## Appendix B

### Derivation of Hydraulic Diameters as Functions of Pitch and Diameters of Fuel Pins

Refer to Fig 1.1 for finding fuel volume fractions, $V_f'$:

$$(V_f')_h = \frac{2\pi d_p^2/4}{6\frac{1}{2}p\frac{p}{2}\sqrt{3}} = \frac{\pi d_p^2}{3\sqrt{3}p_h^2} = \frac{\pi\sqrt{3}}{9}\left(\frac{d_p}{p_h}\right)^2 , \qquad \text{(B-1)}$$

$$(V_f')_t = \frac{\frac{\pi}{2}d_p^2/4}{\frac{1}{2}p\frac{p}{2}\sqrt{3}} = \frac{\pi d_p^2}{2\sqrt{3}p_t^2} = \frac{\pi\sqrt{3}}{6}\left(\frac{d_p}{p_t}\right)^2 , \qquad \text{(B-2)}$$

$$(V_f')_{sq} = \frac{\pi d_p^2/4}{p^2} = \frac{\pi}{4}\left(\frac{d_p}{p_{sq}}\right)^2 . \qquad \text{(B-3)}$$

In the derivations of the linear power output capabilities of the lattices, the assumptions made were that the same fuel pin diameter was to be used in each lattice, and the fuel volume fractions were to be equal. Hence, we obtain the following relations between lattice pitches:

$$(V_f')_h = (V_f')_t ,$$

$$\frac{\pi}{3\sqrt{3}}\left(\frac{d_p}{p_h}\right)^2 = \frac{\pi}{2\sqrt{3}}\left(\frac{d_p}{p_t}\right)^2 ,$$

and

$$p_t^2/p_h^2 = 3/2 . \qquad \text{(B-4)}$$

In like manner

$$p_{sq}^2/p_h^2 = 3\sqrt{3}/4 \qquad \text{(B-5)}$$

By definition $D_e = \dfrac{4 \times \text{cross sectional flow area}}{\text{wetted perimeter}}$ :

$$(D_e)_h = \frac{4(\frac{1}{2}6p_h(p_h/2)\sqrt{3} - 2\pi d_p^2/4)}{2\pi d_p} = \frac{3\sqrt{3}p_h^2 - \pi d_p^2}{\pi d_p}, \qquad \text{(B-6)}$$

$$(D_e)_t = \frac{4(\frac{1}{2}p_t(p_t/2)\sqrt{3} - \frac{1}{2}\pi d_p^2/4)}{\frac{1}{2}\pi d_p} = \frac{2\sqrt{3}p_t^2 - \pi d_p^2}{\pi d_p}. \qquad \text{(B-7)}$$

Using Eq. (B-4),

$$(D_e)_t = \frac{2\sqrt{3}(\frac{3}{2}p_h^2) - \pi d_p^2}{\pi d_p} = (D_e)_h, \qquad \text{(B-8)}$$

$$(D_e)_{sq} = \frac{4(p_{sq}^2 - \pi d_p^2/4)}{\pi d_p} = \frac{4p_{sq}^2 - \pi d_p^2}{\pi d_p}. \qquad \text{(B-9)}$$

Using Eq. (B-5),

$$(D_e)_{sq} = \frac{4(\frac{3\sqrt{3}}{4}p_h^2) - \pi d_p^2}{\pi d_p} = (D_e)_h. \qquad \text{(B-10)}$$

The above results show that for equal pin diameters and fuel volume fractions, the equivalent diameters of the three lattices are equal.

# Appendix C

## Lattice Parameters

Table C.1 lists some of the lattice parameters which are being used in current large LMFBR's and which are proposed for future large LMFBR's. Table C.2 and Fig. C.1 show volume fraction of fuel and triangular lattice pin pitch and gap spacing based on a gap spacing of 0.040 inches for the open-hexagonal lattice (the minimum assumed practical) and equal pin diameters for both lattices.

The equations used in these calculations are Eq. (B-1) and Eq. (B-2). The calculation procedure was to select $d_p$ and, using $\delta_h = 0.040$ inches, compute $p_h$ and $(V_f')_h$ from Eq. (B-1). Then taking $(V_f')_h = (V_f')_t$, $p_t$ and $\delta_t$ are computed from Eq. (B-2) for the same assumed pin diameter. Fig. C.1 shows that as $d_p$ decreases, $\delta_t$ approaches $\delta_h$ with an accompanying drop in $V_f'$. For reasonable pin sizes as shown, and constraints of constant $d_p$ and $V_f'$ between lattices, the following conclusions are drawn:

1. The pin to pin gap for a triangular lattice ( 0.120 in.) is considerably larger than that for an open-hexagonal lattice (0.040 in.).
2. The fuel volume fraction for the lattices with reasonable pin diameters (0.250 to 0.300 inches) are about 0.45 to 0.47. Significant increases above these values require large (and uneconomical) increases in pin diameter.

Table C.1

Current and Proposed LMFBR Parameters

| | A. I.[15A] | B. W.[15B] | C. E.[15C] | G. E.[15D] | W.[15E] |
|---|---|---|---|---|---|
| SYSTEM PARAMETERS | | | | | |
| Electrical power (MWe) | 1004 | 1008 | 1000 | ---- | 1055 |
| Thermal efficiency | 40.7 | 41.2 | 40.6 | ---- | 40.6 |
| Thermal power (MWt) | 2500 | 2450 | 2465 | 2417 | 2600 |
| Inlet temperature ($^{o}$F) | 760 | 800 | 797 | 810 | 770 |
| Outlet temperature ($^{o}$F) | 1060 | 1100 | 1095 | 1150 | 1000 |
| System pressure (psig) | 35 | ---- | ---- | ---- | ---- |
| secondary | 2400 | 2400 | 2400 | ---- | 2446 |
| Flow rate (lb./hr. x $10^{6}$) | 93.0 | 83.8 | 94.0 | ---- | 127.4 |
| CORE AND BLANKET DIMENSIONS | | | | | |
| Core: height (in.) | 50.0 | 34.7 | 24.0 | 30.0 | 40.0 |
| diameter (in.) | 92.5 | 120.0 | 107.0 | 97.4 | 92.5 |
| Blanket: thickness (in.) | ---- | ---- | axial 18.0<br>radial 6.0 | 15.0 | 10.5 |
| Control rods | 15 | ---- | 22 | 31 | 57 |
| NUCLEAR PARAMETERS | | | | | |
| Fuel: enrichment (%) | inner 11.6<br>outer 16.0 | 11.6 | 10.13<br>12.05 | 10.73<br>13.45 | 15.0<br>18.0 |

Table C.1. continued

| | A. I. | B. W. | C. E. | G. E. | W |
|---|---|---|---|---|---|
| Core comp. (vol. %) fuel | 31.0 ($UO_2$) | 44.2 ($UO_2$) | 38.6 (UC) | 46.7 ($UO_2$) | 29.2 |
| sodium/steel | 50.1/18.9 | 35.3/16.9 | 40.0/13.1 | 38.0/14.9 | 52.2/12.5 |
| Critical mass Pu (kg) | 2187 | 2770 | ---- | 1624 fissile | ---- |
| Breeding ratio core/blanket | 0.83/0.49 | 0.93/0.43 | 1.50 | 1.40 | 1.32 |
| Doubling time (yr) | 10.0 | 10.4 | 7.0 | 7.75 | 11.0 |
| Sodium void reactivity ($) | 6.82 | 7.50 | 3.20 | ---- | 10.4 |
| ASSEMBLY PARAMETERS | | | | | |
| Number of pins in core | 56,500 | ---- | 35,700 | ---- | 40,300 |
| Pin diameter/pitch (in/in) | 0.250/0.310 | 0.280/---- | 0.400/0.451 | 0.250/0.300 | 0.302/0.375 |
| Fuel length (in) | 50.0 | ---- | 24.0 | 30.0 | 40.0 |
| Gas plenum length (in) | 64.0 | ---- | ---- | ---- | ---- |
| Axial blanket length (in) | 24 | ---- | 18 | ---- | 15 |
| Pin support method | grid | ---- | wire wrap | undecided | undecided |
| PERFORMANCE PARAMETERS | | | | | |
| Ave. linear power (kWt/ft) | 10.0 | 10.2 | 29.5 | ---- | 18.7 |
| Ave. power density (kWt/l) | 500 | ---- | ---- | ---- | ---- |
| Ave. spec. power (kWt/kg) | 168 | 885 | 121.5 | 1,304 | 168.2 |

Table C.1. continued

| | JAERI[15F] | FFTF[14] | PHENIX[17] | PFR[18] |
|---|---|---|---|---|
| SYSTEM PARAMETERS | | | | |
| Electrical power (MWe) | ---- | ---- | 250 | ---- |
| Thermal efficiency | 40.0 | ---- | ---- | ---- |
| Thermal power (MWt) | 2,500 | 400 | 563 | ---- |
| Inlet temperature ($^{o}$F) | 752 | 600 | 752 | ---- |
| Outlet temperature ($^{o}$F) | 1,166 | 900 | 1,040 | 1040 - 1110 |
| System pressure (psig) primary | ---- | 35 | ---- | ---- |
| secondary | 3,500 | ---- | ---- | ---- |
| Flow rate (lb/hr x $10^{6}$) | 88.4 | ---- | 21.9 | ---- |
| CORE AND BLANKET DIMENSIONS | | | | |
| Core: height (in) | 31.5 | ---- | 33.4 | ---- |
| diameter (in) | 104 | ---- | 53.4 | ---- |
| Blanket thickness (in) | 15.7 | ---- | axial 11.8<br>radial 9.85 | ---- |
| Control rods | 12 | ---- | 6 | ---- |
| NUCLEAR PARAMETERS | | | | |
| Fuel: enrichment (%) | inner 9.5<br>outer 13.0 | ---- | 20.3<br>27.4 | ---- |
| | | | | |

Table C.1. continued

| | JAERI | FFTF | Phenix | PFR |
|---|---|---|---|---|
| Core comp. (vol. %) fuel | 44.2 ($UO_2$) | ---- | 36.8 ($UO_2$) | $UO_2$ |
| sodium/steel | 39.0/16.0 | ---- | 29.7/---- | ---- |
| Critical mass Pu (kg) | total 2,350 fissile 1930 | ---- | 700 | ---- |
| Breeding ratio, core/blanket | 0.96/0.48 | ---- | 0.54/0.62 | ---- |
| Doubling time (yr) | 7.2 | ---- | 17.0 | ---- |
| Sodium void reactivity ($) | 3.1 | ---- | ---- | ---- |
| ASSEMBLY PARAMETERS | | | | |
| Number of pins in core | 89,300 | 16,275 | 11,900 | ---- |
| Pin diameter/pitch (in/in) | 0.250/0.304 | 0.235/0.291 | 0.260/---- | 0.230/---- |
| Fuel length (in) | 31.5 | 36.0 | ---- | 36.0 |
| Gas plenum length (in) | 23.6 | 41.0 | 16.5 | ---- |
| Axial blanket length (in) | 15.75 x 2 | 12.0 | ---- | 18.0 |
| Pin support method | wrapper tube | ---- | spiral wire | grid |
| PERFORMANCE PARAMETERS | | | | |
| Ave. linear power (kWt/ft) | 9.5 | 7.0 | 13.1 | 13.7 peak |
| Ave. power density (kWt/l) | 500 | 386 | 422 | 371 |
| Ave. specific power (kWt/kg) | 1140 | 146 | ---- | 250 peak |

Table C.2

Pin to pin spacing and pin pitch for triangular and open-hexagonal lattices which have equal pin diameters and equal volume fractions of fuel.

| $d_p$ (in.) | $\delta_h$ (in.) | $V_f'$ | $\delta_t$ (in.) | $p_h$ (in.) | $p_t$ (in.) |
|---|---|---|---|---|---|
| 0.25 | 0.040 | 0.450 | 0.105 | 0.290 | 0.355 |
| 0.30 | 0.040 | 0.472 | 0.116 | 0.340 | 0.416 |
| 0.35 | 0.040 | 0.488 | 0.127 | 0.390 | 0.477 |
| 0.40 | 0.040 | 0.501 | 0.138 | 0.440 | 0.538 |
| 0.45 | 0.040 | 0.512 | 0.156 | 0.490 | 0.606 |
| 0.50 | 0.040 | 0.519 | 0.160 | 0.540 | 0.660 |

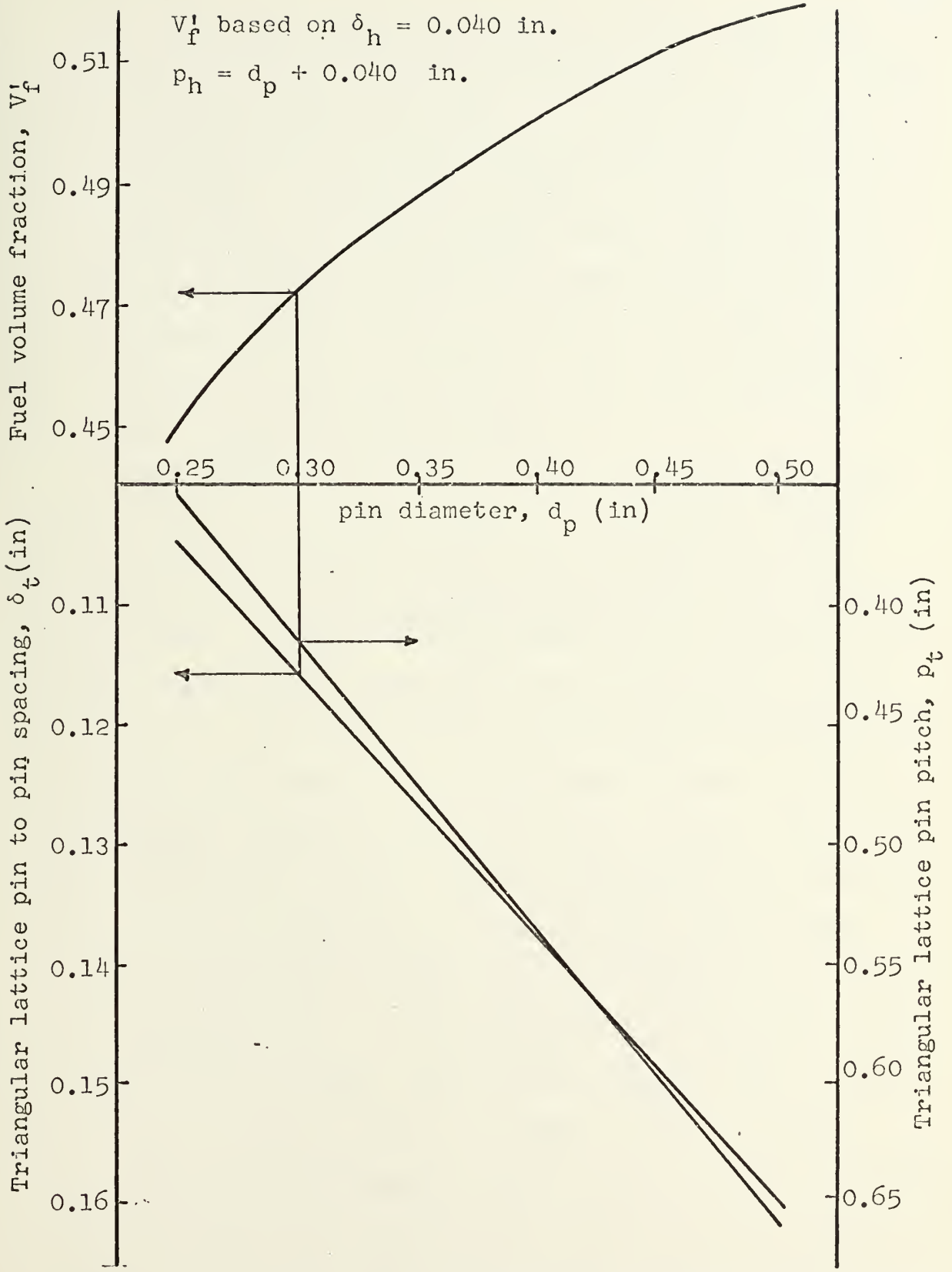


Fig. C.1. Assumed and calculated parameters for the open-hexagonal and triangular lattices.

3. The fuel volume fraction, $V_f'$, used in the above calculations was based on a single fuel cell in a fuel subassembly and was equal to 1 - $V_{Na}$(sodium volume fraction). Taking into account the volume of the core taken up by the clad, the gap between clad and fuel, the subassembly housing, the space between subassemblies, and the control assemblies, the actual fuel volume fraction, $V_f$, for the whole core is 0.306, as will be shown in detail below.

Refer to Fig. C.2 for calculation of the actual core fuel volume fraction, $V_f$. The fuel subassembly contains 217 fuel pins of 0.300 inches outside diameter and has a $V_f'$ of 0.472. Based on a unit length of fuel assembly, the inside volume of the fuel subassembly is $217V_{\text{fuel pin}}/V_f' = 32.2$ in.$^3$. Dividing the subassembly into six equilateral triangles, the height, h, of a triangle becomes one half the internal distance across the flats. Using a wall thickness of 0.150 in. and one half the subassembly to subassembly spacing of 0.025 in., the subassembly pitch divided by two is h' = h + 0.175 in. One equilateral triangle of the subassembly has a volume of $\frac{1}{6}(32.2) = 5.37$ in.$^3$. The volume of one triangle equals $\frac{1}{2}bh = \frac{1}{2}(\frac{2h}{\sqrt{3}})h = \frac{\sqrt{3}}{3}h^2 = 5.37$ in.$^3$ or h = 3.04 in. Now h' = 3.04 + 0.175 = 3.215 in. The volume each subassembly occupies, $V_{SA}$, in the core based on the distance from subassembly center across the flats to the midpoint between subassemblies is $V_{SA} = 6(\frac{1}{2}b'h')$

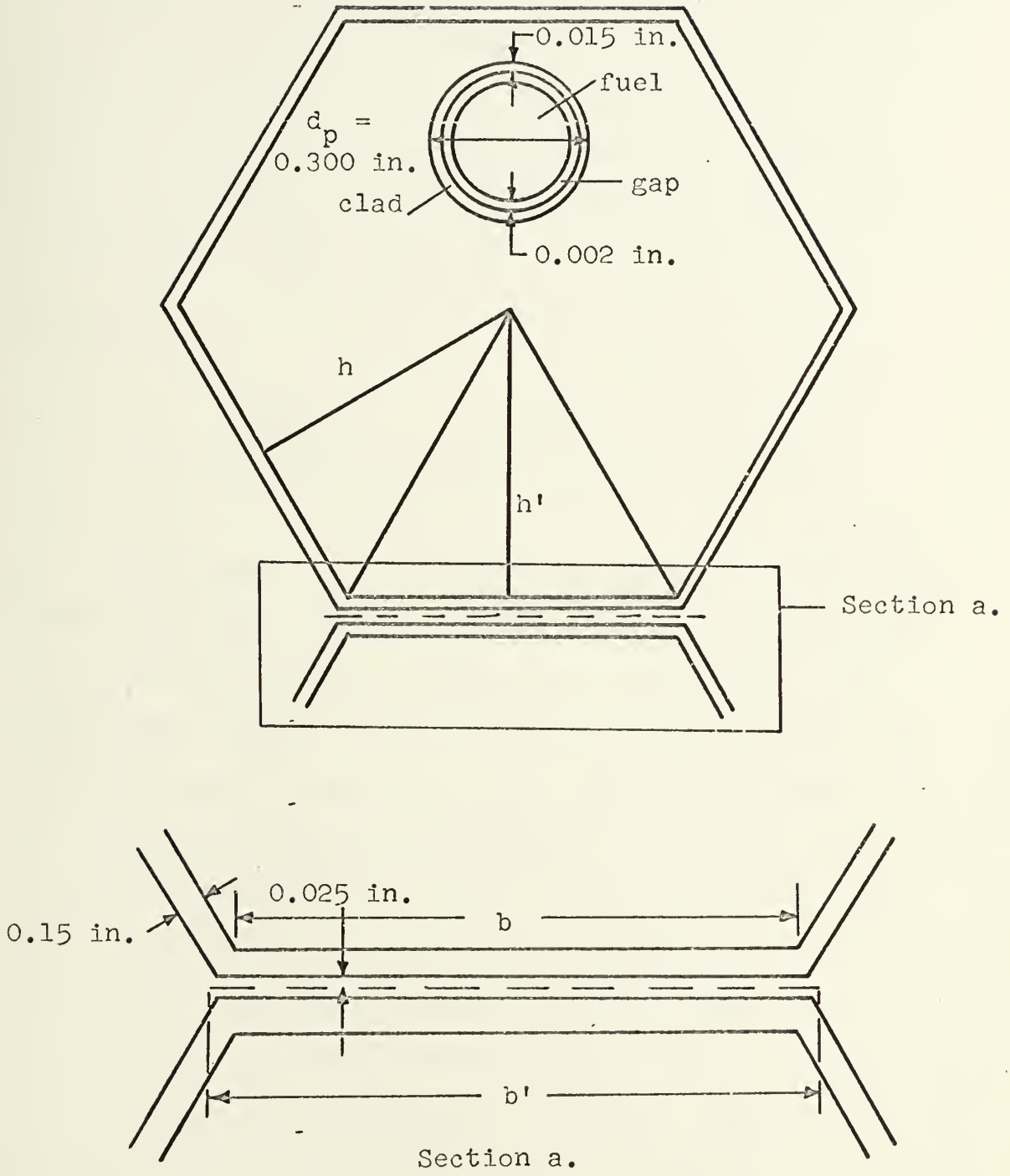


Fig. C.2. Core subassembly configuration

$= 6(\frac{1}{2}(\frac{2\sqrt{3}}{3}h')h') = 2\sqrt{3}h'^2 = 35.75$ in.$^3$. Using a pin diameter of 0.300 in., a clad thickness of 0.015 in., and a fuel to clad radial gap of 0.002 in., the volume of fuel in a subassembly is $V_{fuel} = (217)\frac{\pi(0.300 - 0.034)}{4} = 12.06$ in.$^3$. Assuming there is one control assembly for every ten fuel subassemblies, the actual fuel volume fraction in the core, $V_f$, is

$$V_f = \frac{V_{fuel}}{V_{SA} + \frac{1}{10}V_{SA}} = \left(\frac{12.06}{35.75 + 3.575}\right) = 0.306$$

This number is low compared to the fuel volume fractions ($V_f$ = 29.2 to 46.7) of the reactors in Table C.1. Our value of $V_f$ does not take into consideration the irradiation induced swelling of the stainless steel subassembly walls. Because of this swelling the subassembly to subassembly spacing must be 0.25 inches instead of 0.05 inches. Therefore, $h' = 3.04 + 0.275 = 3.315$ in., and $V_{SA} = 38.07$ in.$^3$. Consequently, our value of $V_f$ is lower: $V_f = 0.288$. The fuel volume fractions of the cores in Table C.1 do not reflect the stainless steel swelling. The methods used to calculate the volumetric compositions of the cores for the reactors in Table C.1 were not explained in the references cited. Therefore, it is difficult to make a good comparison of the volumetric compositions of the actual cores in Table C.1 and our theoretical core. However,

if the $V_f$ of 0.306 is too low for practical use, an increased pin diameter is feasible with the use of uranium carbide fuel which has a higher melting point than does uranium dioxide fuel. Some designs are proposing pin diameters of 0.400 inches for future 1000 Mwe LMFBR's fueled with UC[15c].

Appendix D

## Relative Linear Power Output for Various Lattice Configurations Under Forced Circulation

The average linear power output of a lattice flow cell is given by

$$\overline{q}' = \frac{\overline{\omega} c_p \Delta t}{n_r l} , \qquad \text{(D-1)}$$

where

$$\overline{\omega} = \rho A \overline{V}$$

Assuming the pumps are moving the coolant at the same total rate through the three lattices, and in view of the fact that the volumetric compositions of the three lattices are equal, the coolant velocity will be the same in the three lattices. It is shown in Appendix B that the equivalent diameters of the three lattices are equal. The lattices have the following numbers of effective rods per flow cell: $(n_r)_h = 2$; $(n_r)_t = 1/2$; $(n_r)_{sq} = 1$.

Since

$$A = \frac{D_e \times (\text{wetted perimeter})}{4} , \qquad \text{(D-3)}$$

$$A_h = \frac{D_e(2\pi d_p)}{4} = \frac{D_e \pi d_p}{2} , \qquad \text{(D-4)}$$

$$A_t = \frac{D_e(\frac{1}{2}\pi d_p)}{4} = \frac{D_e \pi d_p}{8} = \frac{1}{\pi} A_h , \qquad \text{(D-5)}$$

$$A_{sq} = \frac{D_e(\pi d_p)}{4} = \frac{1}{2}A_h \quad . \qquad \text{(D-6)}$$

Using the above expressions for flow areas in Eq. (D-2), which is substituted into Eq. (D-1), gives the following relative values for the linear power output of the three lattices:

$$\frac{\overline{q}'_h}{\overline{q}'_t} = \frac{\rho A_h V c_p \Delta t/2l}{\rho A_t V c_p \Delta t/\frac{1}{2}l} = \frac{A_h/2}{\frac{1}{4}A_h/\frac{1}{2}} = 1$$

$$\frac{\overline{q}'_h}{\overline{q}'_{sq}} = \frac{\rho A_h V c_p \Delta t/2l}{\rho A_{sq} V c_p \Delta t/l} = \frac{A_h/2}{A_h/2} = 1$$

$$\frac{\overline{q}'_t}{\overline{q}'_{sq}} = 1$$

The above ratios show that the linear power output for the three lattices are equal under forced circulation for equal $V'_f$ and $d_p$.

The pressure losses through the different lattices are the same since

$$\Delta P = f_F \frac{4l\rho V^2}{D_e 2g_c} \quad , \qquad \text{(D-7)}$$

and all the parameters in Eq. (D-7), including $f_F$ and $D_e$, are equal for the three lattices. The corresponding coolant

velocities, V, are shown to be equal in the lattices in Tables IV.1 and IV.3. The forced convection heat transfer coefficients are also the same for the three lattices since

$$Nu = hD_e/k = C_1 + C_2(Pe)^n,$$

$$Nu = C_1 + C_2(D_e V\rho c_p/k)^n, \qquad (D\text{-}8)$$

and all the values in Eq. (D-8) are again equal for the three lattices, including the $D_e$'s as discussed in Appendix B.

From the above ratios and correlations it is seen that the linear power output, pressure drop, and heat transfer characteristics are the same for the three lattice configurations.

## Appendix E

## References


1. E. B. Ash, "Heat Transfer in Fast Breeder Nuclear Reactors", paper presented at the Education and Creative Engineering Synposium, M.I.T., April, 1969.

2. H. H. Hummel and D. Okrent, Reactivity Coefficients in Large Fast Power Reactors, American Nuclear Society, 1970.

3. C. W. Monroe, Sodium Void Coefficient of Reactivity, a Review and Study of Analytical Work, UNC-2190, United Nuclear Corp., White Plains, New York, May 1965.

4. T. Lacapelle, internal CEA report, June, 1964.

5. P. Benoist, "Théorie du coefficient de diffusion dans un réseau comportant des cavites", CEA report No. 2278, January, 1964.

6. D. J. Behrens, "The Effect of Holes in a Reacting Material on the Passage of Neutrons", Proceeding of the Physical Society of London, 62A: 607, 1949.

7. L. S. Tong, "Pressure Drop Performance of a Rod Bundle", presented at the Winter Annual Meeting of the ASME, New York, New York, December, 1968, Rod Bundle Symposium.

8. A. N. de Stordeur, "Drag Coefficients for Fuel Element Spacers", Nucleonics, Vol. 19, No. 6, June, 1961.

9. W. M. Kays and A. L. London, Compact Heat Exchangers, National Press, Inc., Palo Alto, California, 1955.

10. W. M. Kays, Convective Heat and Mass Transfer, McGraw Hill Book Co., Inc., New York, 1966.

11. R. G. Deissler and M. F. Taylor, TID-7529, Reactor Heat Transfer Conference, New York, pt. 1, book 1, November, 1957.

12. H. Schlichting, Boundary Layer Theory, McGraw Hill Book Co., Inc., New York, 1955.

13. D. J. Bender and P. M. Magee, Turbulent Heat Transfer in a Rod Bundle With Liquid Metal Coolant, GEAP-10052, AEC Research and Development Report, July, 1969.

14. N. E. Todreas, MIT, private communication.

15A* Atomics International, 1000-MWe LMFBR Follow-on Study, November, 1968.

15B* Babcock and Wilcox, 1000-MWe LMFBR Follow-on Study, November, 1968.

15C* Combustion Engineering, Inc., 1000-MWe LMFBR Follow-on Study, November, 1968.

15D* General Electric Co., 1000-MWe LMFBR Follow-on Study, November, 1968.

15E* Westinghouse Electric Corp., 1000-MWe LMFBR Follow-on Study, November, 1968.

15F* Japan Atomic Energy Research Institute, JAERI Presentation, November, 1968.

16. C. F. Bonilla, "Heat Removal", Nuclear Engineering, C. F. Bonilla, ed., McGraw Hill Book Co., Inc., New York, 1957.

17. USAEC, TID-4500, Phenix, Prototype Fast-Neutron Nuclear Power Station, AEC-tr-7130, February, 1970.

18. P. V. Evans, ed., Fast Breeder Reactors, Proceedings of the London Conference on Fast Breeder Reactors, British Nuclear Energy Society, May, 1966, Pergamon Press, New York, 1967.

---

* References (15A) through (15F) were presented at the International Conference on Sodium Technology and Large Fast Reactor Design, Argonne National Laboratory, ANL-7520, November, 1968.

## Appendix F

### Nomenclature
(unless defined as they appear)

| English | Meaning | Units |
|---|---|---|
| A | cross sectional flow area | $ft^2$, $in.^2$ |
| $c_p$ | heat capacity | BTU/lb-$^oF$ |
| d,D | diameter | ft, in. |
| f | friction factor | ---- |
| $g_c$ | gravitational constant | $ft/hr^2$ |
| h | heat transfer coefficient | BTU/hr-$ft^2$-$^oF$ |
| k | thermal conductivity | BTU/hr-ft-$^oF$ |
| k | multiplication factor | ---- |
| l | length | ft, in. |
| n | a quantity | ---- |
| N | pipe length | ft |
| Nu | Nusselt number | ---- |
| $\bar{q}$ | average power output per cell | kw |
| $\bar{q}'$ | average linear power output per pin | kw/ft |
| p | pitch | in. |
| P | perimeter | in. |
| Pe | Peclet number | ---- |
| $\Delta P$ | pressure drop | $lb/ft^2$, psi |
| r | radius | in. |
| Re | Reynolds number | ---- |
| S | cross sectional flow area | $ft^2$, $in.^2$ |

| English | Meaning | Units |
|---|---|---|
| $\Delta t$ | axial temperature difference per cell (inlet to outlet) | $^{o}F$ |
| $\overline{V}$ | average coolant velocity | ft/hr |
| $V_f'$ | fuel volume fraction = 1 - $V_{Na}$ where $V_{Na}$ is the sodium volume fraction | ---- |
| $V_f$ | Actual fuel volume fraction in a real core | ---- |
| z | height | ft |
| Z | elevation difference | ft |

Greek

| | | |
|---|---|---|
| $\beta$ | fraction of delayed neutrons | ---- |
| $\beta$ | temperature coefficient of volumetric expansion | $^{o}F^{-1}$ |
| $\delta$ | pin to pin spacing | in. |
| $\delta$ | boundary layer thickness | in. |
| $\mu$ | dynamic viscosity | lb/ft-hr |
| $\nu$ | kinematic viscosity | $ft^2/hr$ |
| $\rho$ | density | $lb/ft^3$ |
| $\sigma$ | ratio of areas, $A_2/A_1$ | ---- |
| $\overline{\omega}$ | average mass flow rate per flow cell | lb/hr |

Subscripts

| | |
|---|---|
| B | due to buoyancy forces |
| e | equivalent |
| em | empirical |
| E | entrance, exit |

| Subscripts | Meaning |
|---|---|
| g | grids |
| h | open-hexagonal lattice |
| hy | hydraulic |
| p | pin |
| r | rods |
| R | due to friction |
| s | spacers |
| SA | subassembly |
| sq | square |
| t | triangular lattice |
| th | theoretical |
| T | total |
| W | wetted |
| 1 | away from gridded region |
| 2 | in gridded region |

7 DEC 73 22331

Thesis
N469 Newton 120495

Relative performance of different LMFBR lattice configurations under natural circulation.

8 DEC 70
7 DEC 73 DISPLAY 22331

Thesis
N469 Newton 120495

Relative performance of different LMBR lattice configurations under natural circulation.

thesN469
Relative performance of different LMFBR
3 2768 001 89949 5
DUDLEY KNOX LIBRARY